© 2022. Published by The Company of Biologists Ltd | Journal of Cell Science (2022) 135, jcs258937. doi:10.1242/jcs.258937

RESEARCH ARTICLE

Expression analysis and function of mitochondrial genome-encoded microRNAs

Raviprasad Kuthethur[1], Vaibhav Shukla[1], Sandeep Mallya[2], Divya Adiga[1], Shama Prasada Kabekkodu[1], Lingadakai Ramachandra[3], P. U. Prakash Saxena[4], Kapaettu Satyamoorthy[1] and Sanjiban Chakrabarty[1,*]

ABSTRACT

MicroRNAs (miRNAs) play a significant role in nuclear and mitochondrial anterograde and retrograde signaling. Most of the miRNAs found inside mitochondria are encoded in the nuclear genome, with a few mitochondrial genome-encoded non-coding RNAs having been reported. In this study, we have identified 13 mitochondrial genome-encoded microRNAs (mitomiRs), which were differentially expressed in breast cancer cell lines (MCF-7, MDA-MB-468 and MDA-MB-231), non-malignant breast epithelial cell line (MCF-10A), and normal and breast cancer tissue specimens. We found that mitochondrial DNA (mtDNA) depletion and inhibition of mitochondrial transcription led to reduced expression of mitomiRs in breast cancer cells. MitomiRs physically interacted with Ago2, an RNA-induced silencing complex (RISC) protein, in the cytoplasm and inside mitochondria. MitomiRs regulate the expression of both nuclear and mitochondrial transcripts in breast cancer cells. We showed that mitomiR-5 targets the *PPARGC1A* gene and regulates mtDNA copy number in breast cancer cells. MitomiRs identified in the present study may be a promising tool for expression and functional analysis in patients with a defective mitochondrial phenotype, including cancer and metabolic syndromes.

This article has an associated First Person interview with the first author of the paper.

KEY WORDS: Mitochondria, MicroRNAs, MitomiR, *PPARGC1A*, mtDNA copy number

INTRODUCTION

MicroRNAs (miRNAs) are small (18–23 nucleotide) regulatory non-coding RNAs that impact mRNA expression by post-transcriptional regulation in all eukaryotes (Ambros, 2004). Most of the reported miRNAs are encoded in the nuclear genome, processed in the cytoplasm to form a mature miRNA, and loaded into RNA-induced silencing complexes (RISCs) to execute their functions. miRNAs have also been identified and studied in subcellular organelles such as mitochondria. They are translocated from the cytoplasm to regulate mitochondrial functions and target mRNAs in a tissue-specific fashion and under certain pathological conditions (Bandiera et al., 2013; Bienertova-Vasku et al., 2013; Goud and Hua, 2015). Although the mechanism of nuclear miRNA transport into mitochondria is still being identified, miRNAs are known to alter both mitochondrial structure and function, notably biogenesis, bioenergetics and dynamics (Das et al., 2012, 2014; Fan et al., 2019; Favaro et al., 2010; Kren et al., 2009; Lee et al., 2017; Li et al., 2010, 2014; Long et al., 2013; Shen et al., 2016; Sripada et al., 2017; Tak et al., 2014; Tomasetti et al., 2014; Yao et al., 2014). Mitochondrial dysfunction is the hallmark of stress signals arising through age-related consequences as well as complex disorders, including cancer. It is associated with metabolic reprogramming, altered oxidative phosphorylation (OXPHOS), reactive oxygen species (ROS) signaling and apoptosis (Vyas et al., 2016). Classical Warburg phenomena explain the metabolic shift of mitochondria from OXPHOS to increased glycolysis in tumor cells leading to tumor evolution and acquisition of metastatic phenotypes (Warburg, 1956). Breast cancer cells being more heterogeneous, harbor distinct mitochondrial metabolic profiles among estrogen receptor (ER)-positive and ER-negative cells. The glycolytic end-product pyruvate enters either anabolic pathways involving lactate fermentation, fatty acid and nucleic acid biosynthesis to favor the synthesis of biomolecules required for active proliferation, or catabolic pathways involving Kreb's cycle followed by mitochondrial OXPHOS to produce energy (Sun et al., 2020). Previous studies indicate that ER-positive cells rely primarily on OXPHOS for energy production. In contrast, triple-negative breast cancer (TNBC) cells (ER-negative) rely on an enhanced glycolytic pathway (Pelicano et al., 2014). Mitochondrial biogenesis is tightly regulated by various signaling pathways affected by essential effector proteins depending on the energy demand and respective tumor micro-environment. AMP-activated protein kinase (AMPK, also known as PRKAA2) signaling plays a vital role in the activation of mitochondrial biogenesis, the activation of which primarily relies on the accumulation of adenosine monophosphate (AMP) and acts as an energy sensor (Marin et al., 2017). AMPK phosphorylates TSC2 and the mTOR binding partner raptor to inhibit the mTOR signaling pathway and mediates tumor-suppressive functions of LKB1 (Gwinn et al., 2008; Luo et al., 2010). Similarly, sirtuins act as energy sensors in cellular metabolism and protect cells against metabolic stresses (Chang and Guarente, 2014). SIRT1 and AMPK act in a positive regulation loop by activating each other during skeletal muscle biogenesis (Cantó et al., 2009; Fulco et al., 2008; Lan et al., 2008). Conversely, calcineurin-dependent retrograde signaling activated by the reduction in mitochondrial DNA (mtDNA) content activates the epithelial-to-mesenchymal transition (EMT) and generates breast cancer stem cells in human mammary epithelial cells (Guha et al., 2014). All these signaling

[1]Department of Cell and Molecular Biology, Manipal School of Life Sciences, Manipal Academy of Higher Education, Manipal, Karnataka, 576104, India. [2]Department of Bioinformatics, Manipal School of Life Sciences, Manipal Academy of Higher Education, Manipal, Karnataka, 576104, India. [3]Department of Surgery, Kasturba Medical College, Manipal Academy of Higher Education, Manipal, Karnataka, 576104, India. [4]Department of Radiation Oncology, Kasturba Medical College, Manipal Academy of Higher Education, Mangalore, Karnataka, 575001, India.

*Author for correspondence (sanjiban.c@manipal.edu)

R.K., 0000-0003-0697-7835; S.C., 0000-0002-6018-8098

Handling Editor: Michael Way
Received 21 May 2021; Accepted 11 March 2022

Journal of Cell Science (2022) 135, jcs258937. doi:10.1242/jcs.258937

molecules modulated by various cellular factors, including mitochondrial secondary metabolites and deregulated non-coding RNAs, are also known to participate in the carcinogenesis and induction of metastasis (Huang et al., 2018). Recently, long non-coding RNAs (lncRNAs) and mitochondrial DNA-encoded small non-coding RNAs (mitosRNAs) reported to be encoded by mtDNA are believed to regulate mitochondrial functions, and their abnormal expression may participate in diseases by altering the retrograde and anterograde signaling (Vendramin et al., 2017).

Using deep sequencing and parallel analysis of RNA ends (PARE) of purified human mitochondria, Mercer et al. (2011) have identified several small and antisense RNAs generated by the mitochondrial genome and predicted its potential in regulating mitochondrial functions along with nuclear proteins to augment mitochondrial transcription. Antisense non-coding mitochondrial RNAs (ASncmtRNA-2), transcribed from mtDNA during replicative senescence, act as a non-canonical precursor of hsa-miR-4485 and hsa-miR-1973 (Bianchessi et al., 2015). miR-4485, encoded by the nuclear mitochondrial pseudogene *MTRNR2L8* (16S rRNA like 8), also shows sequence similarity to the mitochondrial genome and is involved in the G2-M phase cell cycle arrest during replicative senescence in endothelial cells (Bianchessi et al., 2015). It has also been shown to regulate tumorigenesis in breast cancer cells by regulating the expression of mitochondrial genes and functions (Sripada et al., 2017). The lncRNA *SAMMSON* promotes tumorigenicity of melanoma cells by modulating cytoplasmic and mitochondrial translation machinery. It interacts with the key ribosomal RNA biogenesis and maturation proteins XRN2 and CARF in the nucleoplasm and cytosol to promote ribosome biogenesis and maturation (Vendramin et al., 2018). In the nucleoplasm, CARF is known to sequester XRN2, an important 5′-3′ exoribonuclease involved in the maturation and turnover of most RNA species. *SAMMSON* promotes the binding of p32, a mitochondrial rRNA processing protein, to CARF in the cytosol and, in turn, favors the entry of XRN2 to nucleoli (Vendramin et al., 2018). This favors aberrant translation assembly in both cytosolic and mitochondrial compartments, thus promoting the tumorigenicity of melanoma cells (Leucci et al., 2016). *In silico* prediction of mitochondria-associated small RNAs has been reported earlier (Shinde and Bhadra, 2015). Other non-coding RNAs like mitosRNAs were reported in mouse and human mitochondria (Ro et al., 2013). A previous study by Rackham et al. (2011) identified non-coding RNAs encoded by mtDNA, which represented about 14% of the mitochondrial transcriptome excluding rRNAs and tRNAs (Rackham et al., 2011). It is also known that the argonaute 2 (Ago2) protein of the RISC complex translocates to mitochondria and participates in miRNA-mediated transcriptional regulation (Bandiera et al., 2011; Zhang et al., 2014). However, differential expression of mitochondrial genome-encoded miRNAs (mitomiRs) in breast cancer cells remains to be reported. Also, there is a lack of conclusive evidence of the regulation of mitochondrial function by mitomiRs and their association with RISC proteins such as Ago2 inside mitochondria. Our study has identified 13 novel mitomiRs differentially expressed in breast cancer cell lines and tissue specimens. We have shown that mitomiRs are associated with the mitochondrial RISC complex proteins and target both nuclear and mitochondrial genome-encoded mRNAs. mitomiR expression is altered due to perturbed mtDNA replication and transcription. MitomiR expression in breast cancer cell lines is correlated with mtDNA copy number, suggesting its role in mitochondrial biogenesis in cancer cells.

RESULTS

In silico analysis of mitomiRs

In silico prediction of mitochondrially encoded miRNAs using miRNAFold, which predicts hairpin structure in the given sequence, provided 49 precursor miRNA sequences from mtDNA. Then, RNAFold, another *ab initio* method, was used to cross-verify the obtained sequences. Precursor sequences obtained from these approaches were tested in a comparative approach by phylogenetic analysis using miREval 2.0 (Fig. 1A). In total, 13 precursor mitomiRs (pre-mitomiRs) were selected as novel mitomiRs, and among them five precursor mitomiRs originated from ribosomal RNAs and the rest originated from the coding mRNA regions (Fig. 1B, Table 1). Precursor and mature sequences are listed in Tables S1 and S2.

Small RNA sequencing

Small RNA-sequencing data from the MCF-10A, MCF-7 and MDA-MB-468 cell lines were aligned to nuclear and mitochondrial genomes (GRCh38). Out of 609,198 aligned reads of MCF-10A, 193,419 aligned to the nuclear genome and 4679 reads aligned to the mitochondrial genome. Of the 561,249 total reads from the MCF-7 cell line, 175,674 reads aligned to the nuclear genome and 5750 reads aligned to the mitochondrial genome. However, out of 845,490 reads from the MDA-MB-468 cell line, 472,515 reads aligned to nuclear genome and 20,376 reads aligned to the mitochondrial genome. Reads aligned to the mitochondrial genome from each of the cell lines were used for differential miRNA expression analysis between the normal breast epithelial cell line MCF-10A, luminal A breast cancer cell line MCF-7 and TNBC cell line MDA-MB-468 (Fig. 1C). Distribution of reads showed that most of the reads mapped to the human mitochondrial genome were enriched in the TNBC cell line MDA-MB-468 (Fig. 1D). The majority of the reads were mapped to heavy (H) strands of human mtDNA in the sense orientation (Fig. 1E, Table 2).

Differential expression of mitomiRs in breast cancer cell lines and tumor tissue specimens

Out of 13 precursor mitomiR sequences, mitomiR-1-3p, mitomiR-2-5p, mitomiR-2-3p, mitomiR-3-3p, mitomiR-4-3p, mitomiR-5-5p and mitomiR-5-3p were selected based on their expression in breast cancer cell lines for validation in tissue samples and cell lines using quantitative reverse transcription PCR (qRT-PCR). The purity of the isolated RNA from cytosol and mitochondria was confirmed using reverse transcription PCR (RT-PCR) with the cytoplasmic and mitochondrial markers *GAPDH* and *MT-CYB*, respectively (Fig. S1). The mitomiR expression profile was predominantly high in the TNBC cell line MDA-MB-468 whereas their expression was significantly lower in the other TNBC cell line MDA-MB-231 (Fig. 1F). Among the mitomiRs, mitomiR-5 was significantly upregulated in MDA-MB-468 cells when compared with MDA-MB-231 cells. The differential expression of mitomiRs among the TNBC cell lines suggests their association with mitochondrial and metabolic requirements in breast cancer, where the MDA-MB-231 cell line harbors high glycolytic and low OXPHOS metabolic properties compared to its counterpart (Pelicano et al., 2014). qRT-PCR-based expression analysis in matched normal and breast tumor tissue specimens showed that mitomiR-5 is overexpressed in tumor tissue specimens (Fig. 2A,B). Interestingly, when we compared the expression of mitomiR-5-5p and mitomiR-5-3p in different grades of breast cancer patients, we observed mitomiR-5 expression was more in grade 1 patients when compared with grade 3 patients (Fig. 2C,D). We also performed mitomiR-5-5p and mitomiR-5-3p expression analysis by qRT-PCR in other cancer cell lines such as

Journal of Cell Science (2022) 135, jcs258937. doi:10.1242/jcs.258937

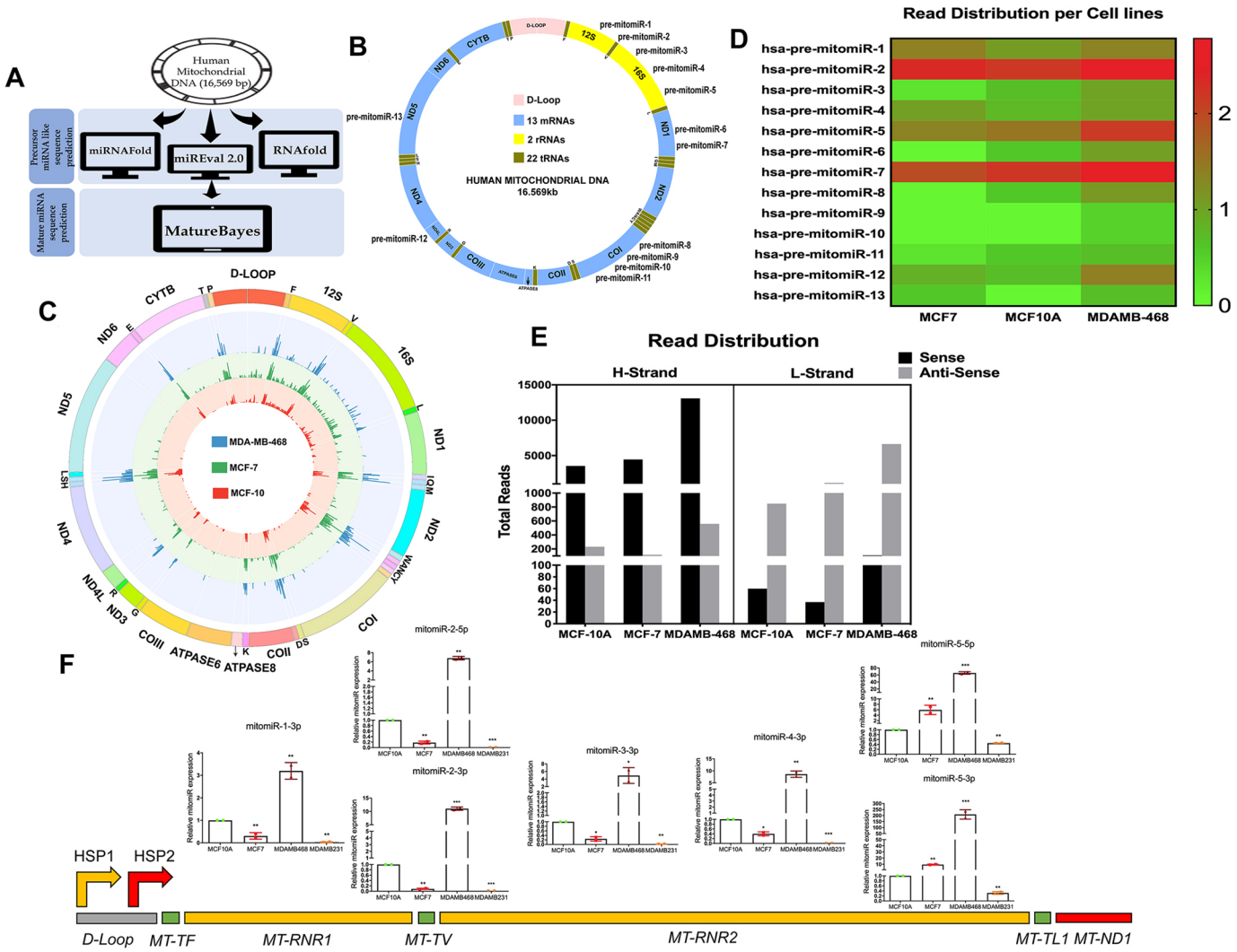

Fig. 1. *In silico* analysis and small RNA sequencing to identify mitochondrial genome-encoded miRNAs. (A,B) Bioinformatic analysis identified 13 mitochondrial genome encoded miRNAs. (C) Circos plot showing the localization of reads aligned to mtDNA of breast cancer cell lines. (D) Heatmap showing the small RNA sequencing read abundance of predicted mitomiRs in breast cancer cell lines MCF-7, MDA-MB-468 and non-malignant MCF-10A cell line. Heatmap was plotted with log values of read counts extracted from each cell line data. Scale on the right side of the figure shows the log scale ranging from 0 to 3, in the order green to red. (E) Small RNA read distribution on heavy (H)- and light (L)-strands in the mitochondrial genome in both sense and antisense directions. (F) Relative quantification of mitomiRs in MCF-7, MDA-MB-468 and MDA-MB-231, compared with the expression levels in MCF10A (n=3). The expression profile of selected mitomiRs are shown, which are arranged according to their position in the mitochondrial genome. 5S rRNA was used as an endogenous control and the relative quantity was calculated using the formula $2^{-\Delta\Delta C_T}$. The P-value was calculated by comparing mitomiR expression levels in breast cancer cell lines against expression levels in MCF-10A as a control sample. *P<0.05, **P<0.001 and ***P<0.0001; comparing expression levels for each mitomiR in individual breast cancer cell lines against expression levels in MCF-10A as a control sample (paired two-tailed Student's t-test).

SiHa, HeLa, CaSki (cervical cancer), PC3 (prostate cancer), HepG2 (hepatocellular cancer), A549 (lung cancer), IMR32, SHSY-5Y (neuroblastoma) and THP1 (leukemia) and compared them with non-cancerous cell lines such as HEK293, primary cells such as fibroblasts and peripheral blood mononuclear cells (PBMCs) (Fig. S2). MitomiR-5-5p and mitomiR-5-3p were found to be differentially expressed in different cell lines, which could be due to the cell type-specific heterogeneity in mitochondrial profile and a possible role of mitomiR-5 in cell type-specific gene regulation (Fig. S2).

MitomiR expression in public datasets

We used publicly available datasets to extend the study cohort of mitomiR expression profiles and compare them with our observations. Small RNA sequencing data comprising different subtypes of breast cancer cell lines, namely MCF-7, MDA-MB-468 and MDA-MB-231, the triple-positive breast cancer cell line BT-474, and the Her2-positive breast cancer cell line SK-BR-3 were examined and compared with the data for MCF-10A and normal human mammary epithelial cells HME1 (Fig. S3A). Interestingly, mitomiR read abundance was found to be more in MCF-7 and MDA-MB-468 compared with other breast cancer cell lines, which was similar to our results from small RNA sequencing and expression analysis by qRT-PCR. Furthermore, to extrapolate the expression profile results to other types of tissues and cancer cell lines, we analyzed data from a wide panel of cancer cell lines arising from central nervous system (CNS) cancers and neuroblastomas (Lorenzi et al., 2021), as well as mitochondrial small RNA sequencing of osteosarcoma 143B cell lines (Mercer et al., 2011). MitomiR read abundance in mitoplast total RNA sequencing data from 143B cell lines showed higher abundance of mitomiR-5-5p and mitomiR-5-3p reads compared to other mitomiRs (Fig. S3B), whereas CNS cancer cell lines showed higher reads in both

Journal of Cell Science (2022) 135, jcs258937. doi:10.1242/jcs.258937

Table 1. Precursor mitomiR mitochondrial location and coordinates on the mitochondrial genome

Chromosome	mitomiR	Coordinate	Mitochondrial genome location
chrM	hsa-pre-mitomiR-1	1322-1428	12S ribosomal RNA
chrM	hsa-pre-mitomiR-2	1546-1668	tRNA valine and 16S ribosomal RNA
chrM	hsa-pre-mitomiR-3	1915-2042	16S ribosomal RNA
chrM	hsa-pre-mitomiR-4	2564-2655	16S ribosomal RNA
chrM	hsa-pre-mitomiR-5	2912-3041	16S ribosomal RNA
chrM	hsa-pre-mitomiR-6	3875-3936	NADH dehydrogenase subunit 1
chrM	hsa-pre-mitomiR-7	4196-4332	NADH dehydrogenase subunit 1
chrM	hsa-pre-mitomiR-8	6254-6375	Cytochrome c oxidase subunit I
chrM	hsa-pre-mitomiR-9	6621-6755	Cytochrome c oxidase subunit I
chrM	hsa-pre-mitomiR-10	6670-6787	Cytochrome c oxidase subunit I
chrM	hsa-pre-mitomiR-11	6885-6999	Cytochrome c oxidase subunit I
chrM	hsa-pre-mitomiR-12	10,629-10,731	NADH dehydrogenase subunit 4L
chrM	hsa-pre-mitomiR-13	12,725-12,846	NADH dehydrogenase subunit 5

mitomiR-5 and mitomiR-2 reads as observed in our sequencing results (Fig. S3C). Interestingly, brain tissue samples showed heterogeneity in the mitomiR expression profile. The majority of the mitomiR read abundance was high in astrocytes and brain stem cells (Fig. S3D). Among the mitomiRs, mitomiR-5-3p expression was significantly upregulated in astrocytes and brain stem cells, which plays a major role in maintaining mitochondrial bioenergetics and development (Du et al., 2018).

MitomiRs are encoded by the mitochondrial genome

Exposure to 2′,3′-dideoxycytidine (DDC) and ethidium bromide (EtBr) leads to depletion of mitochondrial DNA and downregulation of mitochondrial genome encoded transcripts (Kao et al., 2012; Torregrosa-Muñumer et al., 2015; Warren et al., 2017). MCF-7 breast cancer cells that were treated with DDC for one passage showed significant decrease in the mtDNA content (Fig. 3A), decreased expression of the mitochondrial transcript *MT-CO2* (Fig. 3B) and decreased expression of mitomiR-5-5p and mitomiR-5-3p (Fig. 3C). EtBr treatment for 6 h did not reduce the levels of mtDNA (Fig. 3D), whereas it significantly reduced the levels of the mitochondrial transcript *MT-CO2* (Fig. 3E) and decreased expression of mitomiR-5-5p and mitomiR-5-3p (Fig. 3F). The nuclear genome-encoded miRNA, hsa-miR-200b, which served as a control in the DDC and EtBr treatment experiments, did not show any change in the expression levels (Fig. 3C,F). These data collectively suggest that mtDNA depletion can lead to mitomiR downregulation.

Transcription factor A, mitochondria (TFAM) is a known regulator of mitochondrial gene transcription and recruits mitochondrial DNA-directed RNA polymerase (POLRMT) along with transcription factor B2, mitochondrial (TFB2M) to the mitochondrial promoter to initiate transcription (Ramachandran et al., 2017). TFAM is also known to be associated with mtDNA replication (Pohjoismäki et al., 2006). TFAM knockdown (KD) cells showed reduced TFAM protein expression (Fig. 3G), decreased mtDNA copy number (Fig. 3H) and mitochondrial mass (Fig. 3I). qRT-PCR analysis of mitomiR-5-5p in control and TFAM KD cells showed a significant decrease in mitomiR-5-5p expression, further confirming our observation that mtDNA depletion leads to mitomiR downregulation (Fig. 3J). These data suggest that the mitomiRs predicted in our study are encoded by the mitochondrial genome and perturbed mtDNA replication and transcription can alter mitomiR transcript levels. We observed that the mitochondrial respiratory complex inhibitor antimycin A (complex III inhibitor) (Reda et al., 2019) and tetracycline (inhibits mitochondrial translation, induces proteotoxic stress and inhibits nuclear-mitochondrial communication) (Moullan et al., 2015) significantly reduced mitomiR-5-5p and mitomiR-5-3p expression (Fig. 3K,L). Dose-dependent treatment of the mitochondrial OXPHOS inhibitor antimycin A from sub-lethal (25 nM) to IC50 (100 nM) concentrations showed a gradual reduction in the mitomiR-5 expression, suggesting that the functional alteration of mitochondria can regulate mitomiR-5 expression. Tetracycline treatment is known to induce proteotoxic stress by inducing mitochondria-nuclear protein transport imbalance. This could possibly indicate the role of nuclear genome-encoded mitochondrial proteins in the transcription and biogenesis of mitomiRs (Moullan et al., 2015). Nuclear miRNA-146a served as a positive control, which is known to be inhibited during mitochondrial dysfunction (Su et al., 2021).

MitomiR-5-5p and mitomiR-5-3p binds to Ago2 protein inside mitochondria

To confirm the mitochondrial localization and intracellular distribution of mitomiR-5, immunofluorescence imaging of biotinylated mitomiR-5-5p mimic-transfected cells and co-staining

Table 2. Mapping of small RNA reads to mitochondrial genome of breast cancer cell lines

Cell lines	Strand	Orientation	Total mitomiRs	tRNAs	rRNAs	mRNAs	D-loop
MCF-10A (4679)	H (80.59%)	Sense	3539	2650	697	142	50
		Antisense	232	7	1	136	88
	L (19.40%)	Sense	60	57	0	3	0
		Antisense	848	848	0	0	0
MCF-7 (5750)	H (97.6%)	Sense	4450	3762	491	172	25
		Antisense	117	6	1	50	60
	L (2.39%)	Sense	37	37	0	0	0
		Antisense	1146	1146	0	0	0
MDA-MB-468 (20376)	H (66.98%)	Sense	13,090	10,404	1724	439	523
		Antisense	559	18	0	280	261
	L (33.01%)	Sense	108	103	0	5	0
		Antisense	6619	6615	0	4	0

Journal of Cell Science (2022) 135, jcs258937. doi:10.1242/jcs.258937

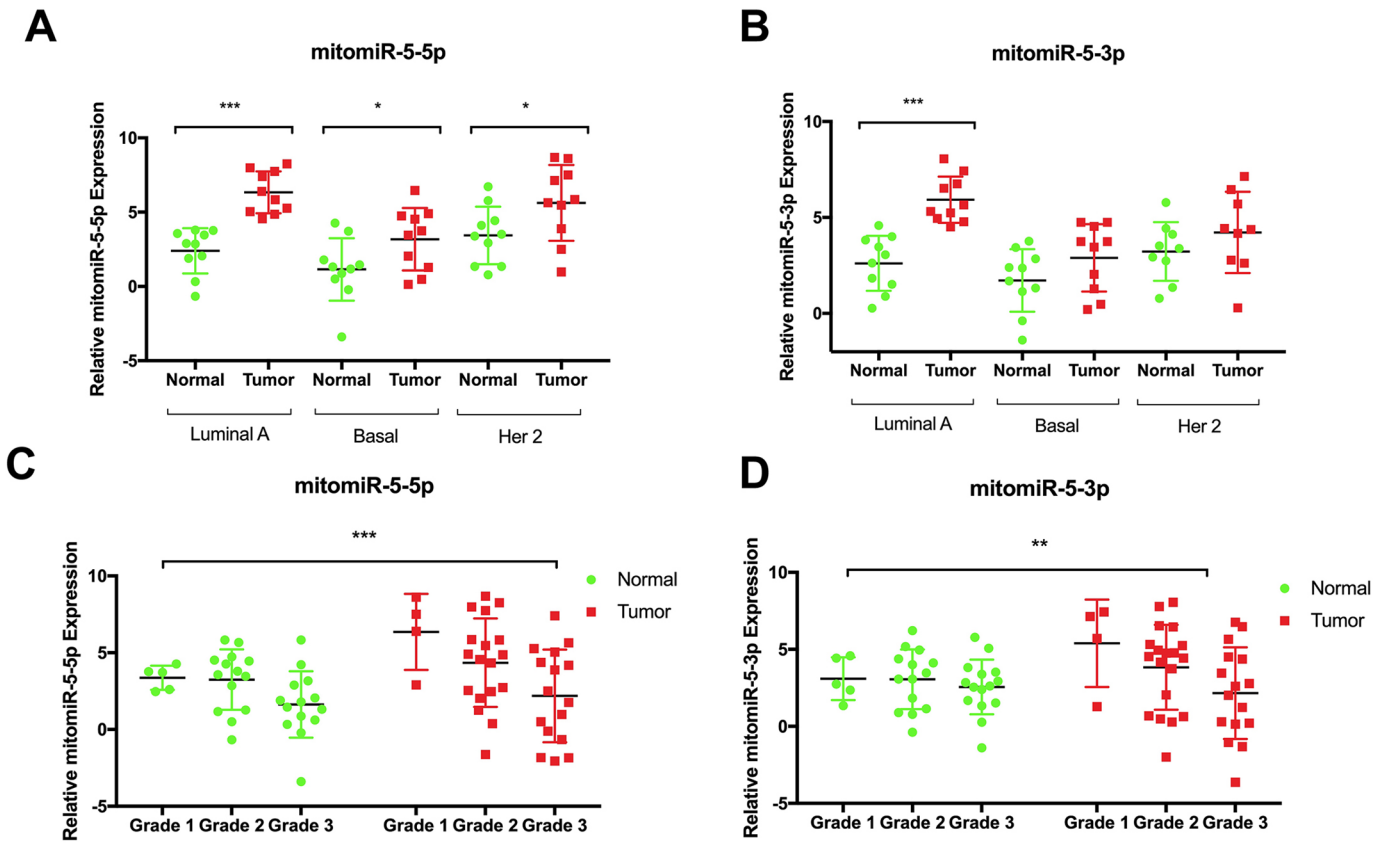

Fig. 2. Expression profile of mitomiRs in breast cancer tumor specimens. (A,B) Relative quantification of mitomiR-5-5p (A) and mitomiR-5-3p (B) in matched normal and breast cancer patient tumor tissue specimens with different subtypes which includes luminal A (*n*=20), TNBC (*n*=20) and Her2-positive breast cancer (*n*=20). (C,D) mitomiR-5-5p (C) and mitomiR-5-3p (D) expression profiles in breast cancer patients with different tumor grades. *RNU6B* served as an endogenous control and the relative quantity was calculated using the formula $2^{-\Delta C_T}$. **P*<0.05, ***P*<0.001 and ****P*<0.0001; between different subtypes of normal and tumor breast cancer specimens (paired two-tailed Student's *t*-test) or between different grades of normal and tumor breast cancer specimens (two-way ANOVA with Tukey HSD post-hoc test).

with MitoTracker Red was performed. Immunofluorescence staining followed by confocal microscopy showed that mitomiR-5-5p is predominantly localized to mitochondria (Fig. 4A). To elucidate the mitomiR-5-5p and mitomiR-5-3p interaction with RISC complex proteins inside mitochondria, Ago2 immunoprecipitation (IP) was performed in pure mitoplast fractions isolated from the breast cancer cell line MDA-MB-468. To confirm the association of mitomiRs with mitochondrial Ago2, we cloned the Ago2 full length coding sequence (CDS) region into the pCMV/myc/mito plasmid between the Sal1 and Not1 sites within the multiple cloning site (MCS) to generate a fusion protein with an N-terminal mitochondrial translocation signal (MTS) and a C-terminal myc tag. To ensure the specificity and direct effect of mitomiR-5 downregulation on Ago2 and mitomiR-5 binding, we performed Ago2 IP in TFAM KD cell lines. The presence of Ago2 in the mitochondrial fraction was confirmed by immunoblotting (protein) along with mitochondrial markers (Fig. 4B). Expression of exogenous Ago2 in the mitochondrial compartment was confirmed using myc-tag antibody along with a mitochondrial marker (Fig. 4C). qRT-PCR analysis for mitomiR-5-5p and mitomiR-5-3p expression in the Ago2 IP- and IgG IP-eluted RNA for both the cytoplasmic fractions (800-fold) and mitochondrial fractions (3000-fold) showed that mitomiRs physically interact with the Ago2 protein (Fig. 4D). The qRT-PCR amplification products of mitomiRs were visualized on agarose gels to ensure the size of the amplicon (Fig. 4E). Similarly, IP was performed from whole-cell lysates of Ago2/myc/mito-transfected cells and TFAM KD cells using the myc-tag antibody and Ago2 antibody, respectively. Myc–Ago2 IP showed a significant enrichment of mitomiR-5 compared with the empty control, suggesting the direct interaction of mitochondrial Ago2 protein with mitomiR-5 (Fig. 4F,G). The levels of the nuclear miRNA hsa-miR-146a were also analyzed in the Myc–Ago2 IP elute as a positive control, as miR-146a translocates to mitochondria (Fig. S6) (Su et al., 2021). Ago2 IP with TFAM KD cells showed reduced levels of mitomiR-5 in TFAM KD cells compared with the scrambled control group (Fig. 4H). These data suggest that mitomiR-5 physically interacts with the mitochondrial RISC complex protein Ago2 and is present as canonical microRNA inside mitochondria. We measured the abundance of the mitomiR-5 target genes (described in Fig. 5) *PPARGC1A*, *MT-CO1* and *MT-CO2* using the RNA eluted from Ago2 IPs in both cytoplasmic and mitochondria fractions to confirm their interaction with mitomiR-5. We observed that *PPARGC1A* abundance was predominant in the cytoplasmic fraction (Fig. 4I) whereas *MT-CO1* and *MT-CO2* abundance was predominant in the mitochondrial fraction (Fig. 4J,K). These results suggested that mitomiR-5-5p and mitomiR-5-3p physically interact with the Ago2 protein associated with the RISC complex both in the cytoplasm and inside mitochondria.

MitomiR-5-5p target mitochondrial genes

Multiple sequence alignment of mitomiR-5-5p and mitomiR-5-3p showed a conserved seed region (Fig. S4). We confirmed mitomiR-5-5p expression after transfecting chemically modified RNA

Journal of Cell Science (2022) 135, jcs258937. doi:10.1242/jcs.258937

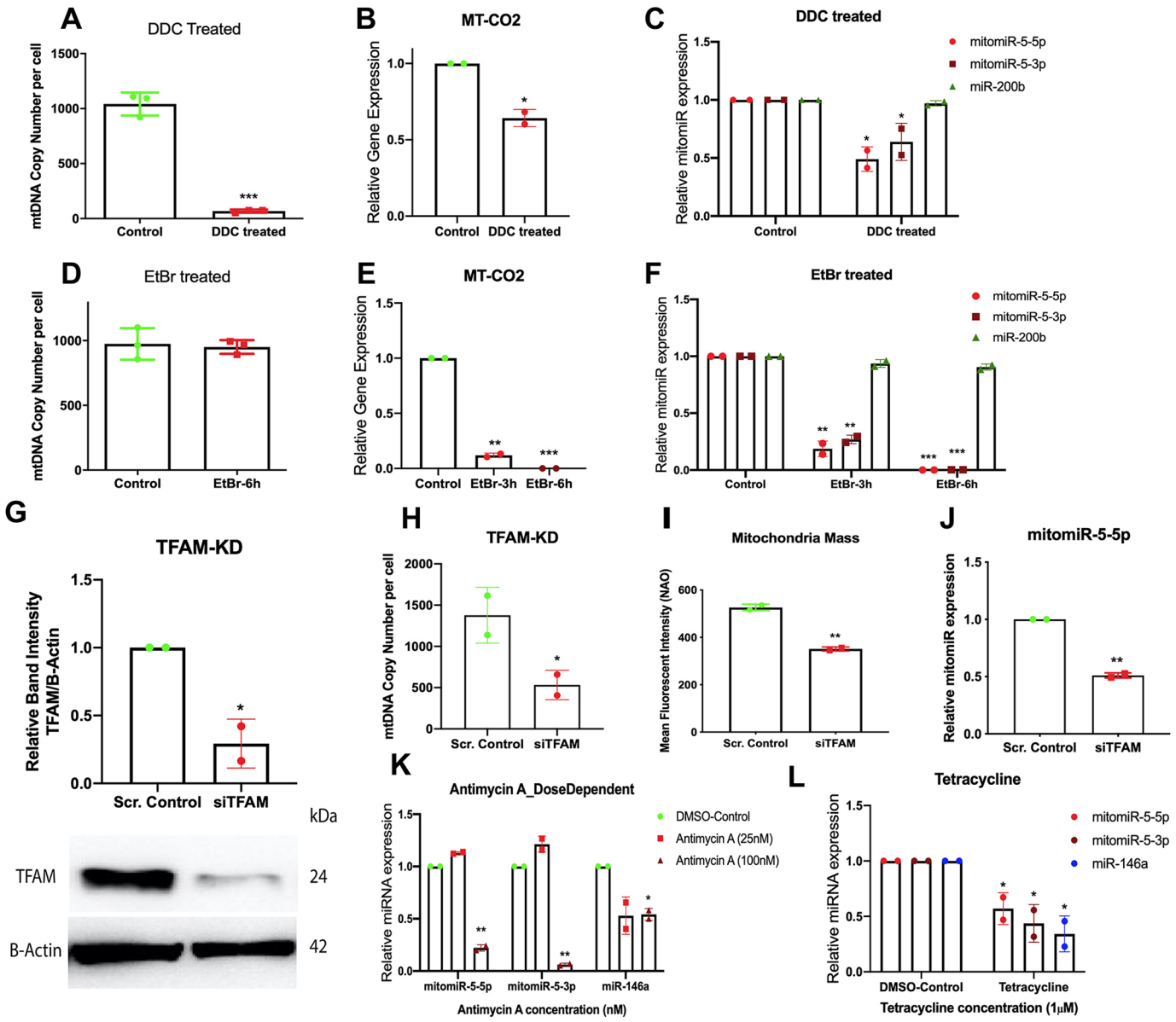

Fig. 3. MitomiRs are encoded by the mitochondrial genome. Mitochondrial DNA depletion and transcription inhibition using 2′,3′-dideoxycytidine (DDC) (2 µM) for one passage with supplements and ethidium bromide (EtBr) (50 ng/ml) for 3 and 6 h were performed using the MCF-7 cell line. Mitochondrial DNA copy number, mitochondrial transcript expression, mitomiR and nuclear miRNA expression analyses were performed by qRT-PCR. (A) mtDNA copy number analysis in DDC-treated cells. (B) Expression analysis of *MT-CO2* in control and DDC-treated cells. (C) Expression analysis of mitomiR-5-5p, mitomiR-5-3p and miR-200b (nuclear miRNA) in control and DDC-treated cells. (D) mtDNA copy number analysis in EtBr-treated cells. (E) Expression analysis of *MT-CO2* in control and EtBr-treated cells. (F) Expression analysis of mitomiR-5-5p, mitomiR-5-3p and miR-200b (nuclear miRNA) in EtBr-treated cells. (G) Western blot analysis showing the protein levels of TFAM in scramble (scr.) control and TFAM KD (siTFAM) cells. (H,I) Validation of TFAM KD cells in comparison with scramble control cells by mtDNA copy number analysis (H) and mitochondrial mass analysis (I). (J) MitomiR-5-5p expression analysis in control and TFAM KD cells. (K,L) MitomiR-5 expression analysis in antimycin A-treated (K) and tetracycline-treated (L) MCF-7 cells. miR-146a served as a positive control. β-actin served as an endogenous control for gene expression, and RNU6B served as an endogenous control for all the miRNA expression analysis. Relative quantity (RQ) was calculated using the formula $2^{-\Delta C_T}$ for mtDNA copy number, and the formula $2^{-\Delta\Delta C_T}$ was used for gene and miRNA expression. n=3. *P<0.05, **P<0.001 and ***P<0.0001 between each control and test sample (paired two-tailed Student's t-test) or between control (DMSO) and mitochondrial inhibitor (antimycin A and tetracycline)-treated groups (two-way ANOVA with Tukey HSD post-hoc test).

molecules that either mimic the expression of endogenous mitomiRs in MDA-MB-468 cells or inhibit the interaction between mitomiR and the target genes by competitive interaction with the mitomiR-5-5p seed region (Fig. S5). The *PPARGC1A* gene, that encodes PPARGC1α, a mitochondrial transcriptional cofactor, was identified as a putative direct target of mitomiR-5-5p (Fig. 5A; Table S3). Bioinformatic analysis identified that mitomiR-5-5p also targets the mtDNA encoding *MT-CO1* and *MT-CO2* (Fig. 5B,C). Dual luciferase reporter assay showed that mitomiR-5-5p mimic repressed the *PPARGC1A*, *MT-CO1* and *MT-CO2* reporter activity whereas the mutant construct co-transfected with mitomiR-5-5p mimic did not show any change in the luciferase activity, suggesting that mitomiR-5-5p directly targets its target genes *PPARGC1A*, *MT-CO1* and *MT-CO2* (Fig. 5D–F). We also observed that mitomiR-5-5p mimic-transfected cells had increased *MT-CO1* and *MT-CO2* transcript expression levels (Fig. 5G,H) whereas mitomiR-5-5p

Journal of Cell Science (2022) 135, jcs258937. doi:10.1242/jcs.258937

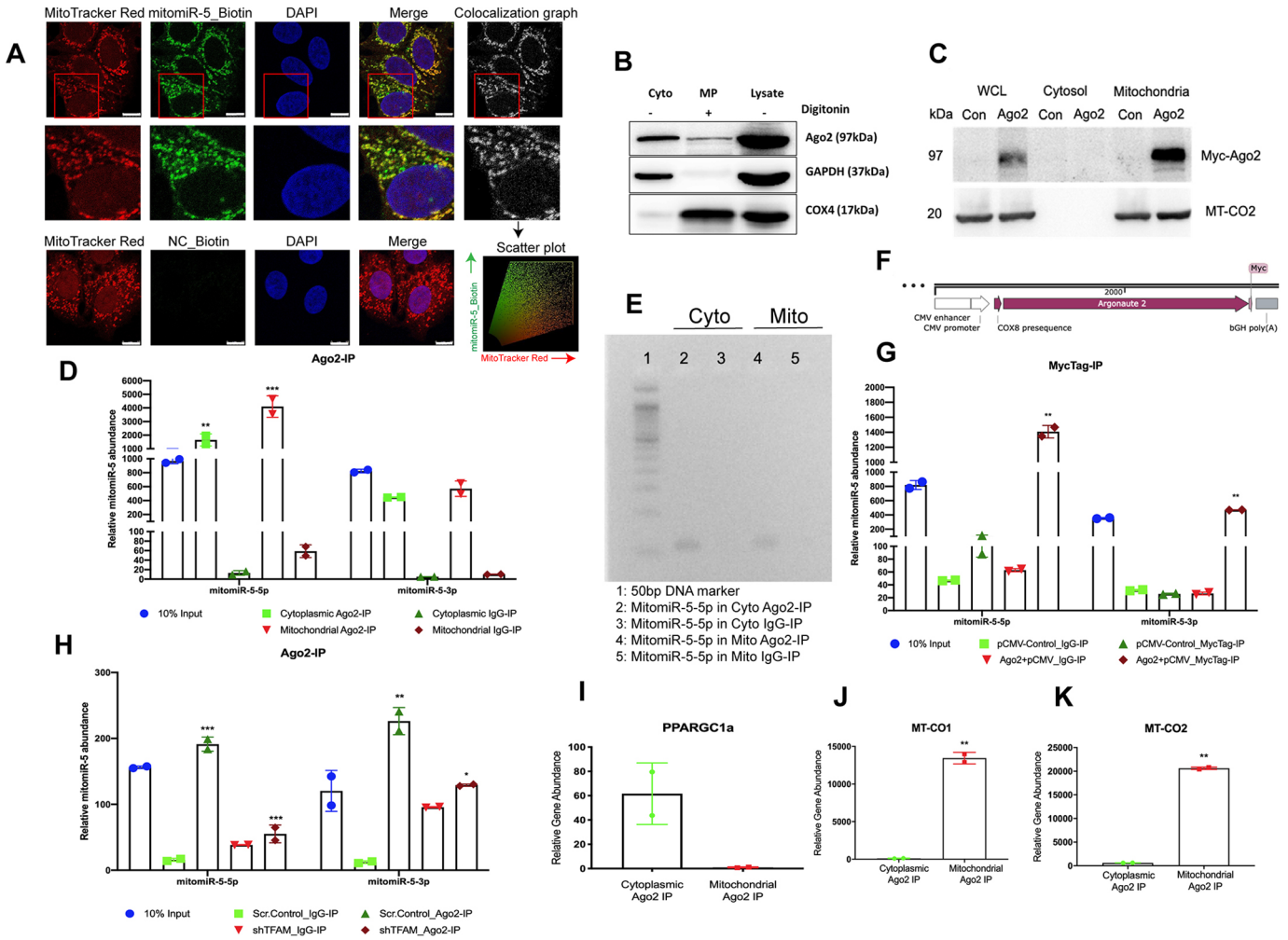

Fig. 4. MitomiR-5-5p and mitomiR-5-3p binds to RISC complex protein. (A) Immunofluorescence imaging of 75 nM biotinylated mitomiR-5 mimics or negative control oligonucleotides stained with streptavidin Alexa Fluor 488, co-stained with MitoTracker Red and DAPI. Images were captured using a 100× oil immersion objective of a confocal fluorescent microscope. Co-localization analysis was performed using LAS X co-localization analysis tool by merging channel 1 (MitoTracker Red) and channel 2 (mitomiR-5-5p). Merged data were extracted to generate a scatter plot showing co-localization of mitomiR-5-5p. Mean Pearson's correlation coefficient was found to be 0.53284. Images are representative of three independent experiments. Scale bars: 10 µm. (B) Detection of Ago2 in the mitoplast (MP) fraction and cytoplasmic (Cyto) fraction. Western blot results showing the cytoplasmic and mitochondrial markers, GAPDH and COX4, respectively, to check the purity of isolated cellular fractions. *n*=3. (C) Western blotting images showing exogenous Ago2 and MT-CO2 expression in the whole cell lysate (WCL), cytoplasmic and mitochondrial fractions prepared from Ago2-transfected MCF-7 cells to confirm the localization of Ago2 protein, probed with anti-myc tag antibody. Con, control. *n*=3. (D) qRT-PCR analysis showing the abundance of mitomiR-5-5p and mitomiR-5-3p in Ago2 elutes of cytoplasmic and mitochondrial fractions. IgG rabbit Ab was used as the experimental control and empty beads (input) were used as the negative control. Fold change was calculated by normalizing the Ago2 IP and IgG IP elute amplification to empty beads amplification. *n*=3. (E) Agarose gel electrophoresis image showing the qRT-PCR amplification products corresponding to mitomiR-5-5p in cytoplasmic and mitochondrial fractions. *n*=3. (F) Schematic representation of cloned Ago2/myc/mito fusion protein with N-terminal mitochondrial translocation signal (MTS, COX8 presequence) and C-terminal myc-tag. (G) qRT-PCR analysis showing the abundance of mitomiR-5 in Ago2/myc/mito-transfected cells compared to control vector transfected cells. Myc-tag IP was performed with the whole cell lysate of both the cell lysates, using mouse IgG IP as experimental control. *n*=3. (H) qRT-PCR analysis showing the abundance of mitomiR-5 in Ago2 IP and IgG IP elutes of scramble control and TFAM KD cells. 10% inputs were kept aside from each of the lysates prior to immunoprecipitation, and served as input control in all the IP experiments. *n*=3. (I–K) Quantification of Ago2-associated nuclear genome-encoded *PPARGC1A* (I) in the cytoplasmic fraction as well as mtDNA-encoded transcripts *MT-CO1* (J) and *MT-CO2* (K) in the mitochondrial fraction by qRT-PCR. Fold change was calculated by normalizing the Ago2 IP amplification to IgG IP amplification. *n*=3. **P*<0.05, ***P*<0.001 and ****P*<0.0001; between IgG-IP and Ago2/MycTag-IP for all the immunoprecipitation experiments or mitomiR-5 abundance among control and test samples of Ago2/myc/mito and TFAM-KD samples (paired two-tailed Student's *t*-test).

inhibitor-transfected cells had reduced *MT-CO1* and *MT-CO2* transcript expression levels when compared to scrambled mimic- and inhibitor-transfected control cells (Fig. 5G,H). We also observed that mitomiR-5-5p mimic-transfected cells have increased MT-CO2 protein expression when compared to scrambled mimic-transfected control cells (Fig. 5I). The *MT-CO1* and *MT-CO2* genes are essential subunits of cytochrome c oxidase, also known as complex IV of the mitochondrial respiratory chain. Spectrophotometric assessment of complex IV activity in mitomiR-5-5p mimic-transfected cells showed a slight increase in activity when compared with mitomiR-5-5p inhibitor-transfected cells (Fig. 5J).

MitomiR-5-5p and mitomiR-5-3p regulate mtDNA copy number

PPARGC1α is a known regulator of mitochondrial biogenesis and oxidative phosphorylation (LeBleu et al., 2014). Gene expression

Journal of Cell Science (2022) 135, jcs258937. doi:10.1242/jcs.258937

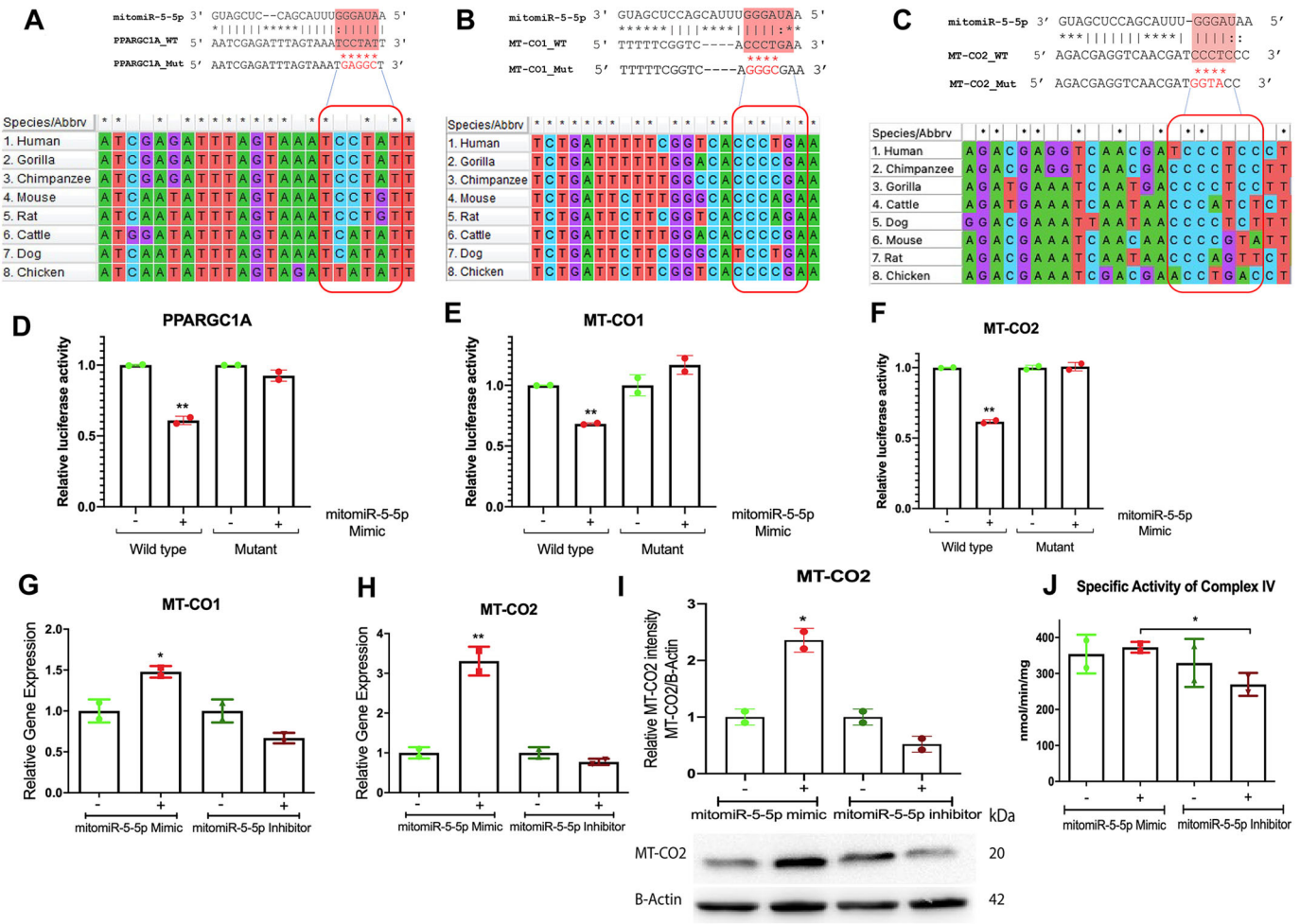

Fig. 5. MitomiR-5-5p targets *PPARGC1A*, *MT-CO1* and *MT-CO2* in breast cancer. (A–C) *In silico* analysis predicted the nuclear gene *PPARGC1A* (A) and mitochondrial genes *MT-CO1* (B) and *MT-CO2* (C) are the putative targets of mitomiR-5-5p. (D–F) Luciferase reporter activity upon co-transfection of target genes cloned in pmirGLO vector with wild-type and mutant constructs along with 50 nM of mitomiR-5-5p mimics or scrambled negative control oligonucleotides in MCF-7 cells for *PPARGC1A* (D), *MT-CO1* (E) and *MT-CO2* (F). Wild-type constructs with mimics showed reduced luciferase activity whereas the mutant constructs with mimics showed no changes to the luciferase activity. *Renilla* luciferase served as an internal control and relative luciferase activities were plotted upon normalization. *n*=3. (G,H) Gene expression analysis *MT-CO1* (G) and *MT-CO2* (H) in MDA-MB-468 cell line upon transfection of 50 nM mitomiR-5-5p mimics and inhibitors, along with the respective control oligonucleotides. *n*=3. (I) Western blot results along with densitometric normalization showing MT-CO2 expression in 75 nM mitomiR-5-5p mimic- and inhibitor-transfected MDA-MB-468 cell line, along with respective control oligonucleotides. The negative signs in the images represent the scrambled mimic control or scrambled inhibitor control oligonucleotides, for all the mimic- and inhibitor-transfected experiments. *n*=3. (J) Complex IV OXPHOS activity upon mitomiR-5-5p mimic and inhibitor transfection. Specific complex IV activity was calculated by normalizing the absorbance between presence and absence of specific complex IV inhibitor: sodium azide. Negative sign in the images represent the scrambled mimic control and scrambled inhibitor control oligonucleotides, for all the mimic and inhibitor transfected experiments. *n*=3. **P*<0.05 and ***P*<0.001; between mimic/inhibitor-treated group and respective control oligo-treated group (paired two-tailed Student's *t*-test).

analysis of *PPARGC1A* showed decreased expression in MDA-MB-468 cells, which correlated with increased mitomiR-5-5p expression in MDA-MB-468 cells (Fig. S7). Interestingly, mitomiR-5-5p expression was low in MDA-MB-231, which correlated with high *PPARGC1A* expression in MDA-MB-231 cells (Fig. S7). We observed that PPARGC1α protein expression was decreased in mitomiR-5-5p mimic-transfected cells when compared to scrambled mimic-transfected control cells (Fig. 6A). Interestingly, cells transfected with mitomiR-5-5p inhibitor showed increased PPARGC1α protein expression when compared to scrambled inhibitor-transfected control cells, suggesting that mitomiR-5-5p directly targets PPARGC1α (Fig. 6A). To understand the effect of mitomiR-5-mediated PPARGC1α downregulation in breast cancer cells, we performed mtDNA copy number analysis in mitomiR-5 mimic- and inhibitor-transfected cells. We observed that mitomiR-5 mimic-transfected cells have decreased mtDNA copy number when compared with scrambled mimic-transfected control cells, and mitomiR-5-5p inhibitor-transfected cells showed increased mtDNA copy number when compared to scrambled inhibitor-transfected control cells (Fig. 6B, C). However, quantitative analysis of mitochondrial mass did not show any significant difference in mitomiR-5 mimic- and inhibitor-transfected cells (Fig. S7). Confocal imaging analysis of mtDNA content in mitomiR-5-5p mimic-transfected cells showed marked decrease in mtDNA content when compared with scrambled mimic-transfected control cells (Fig. 6D). When we transfected the mitomiR-5-5p inhibitor, we were able to restore the mtDNA content which was comparable with that of the scrambled

Journal of Cell Science (2022) 135, jcs258937. doi:10.1242/jcs.258937

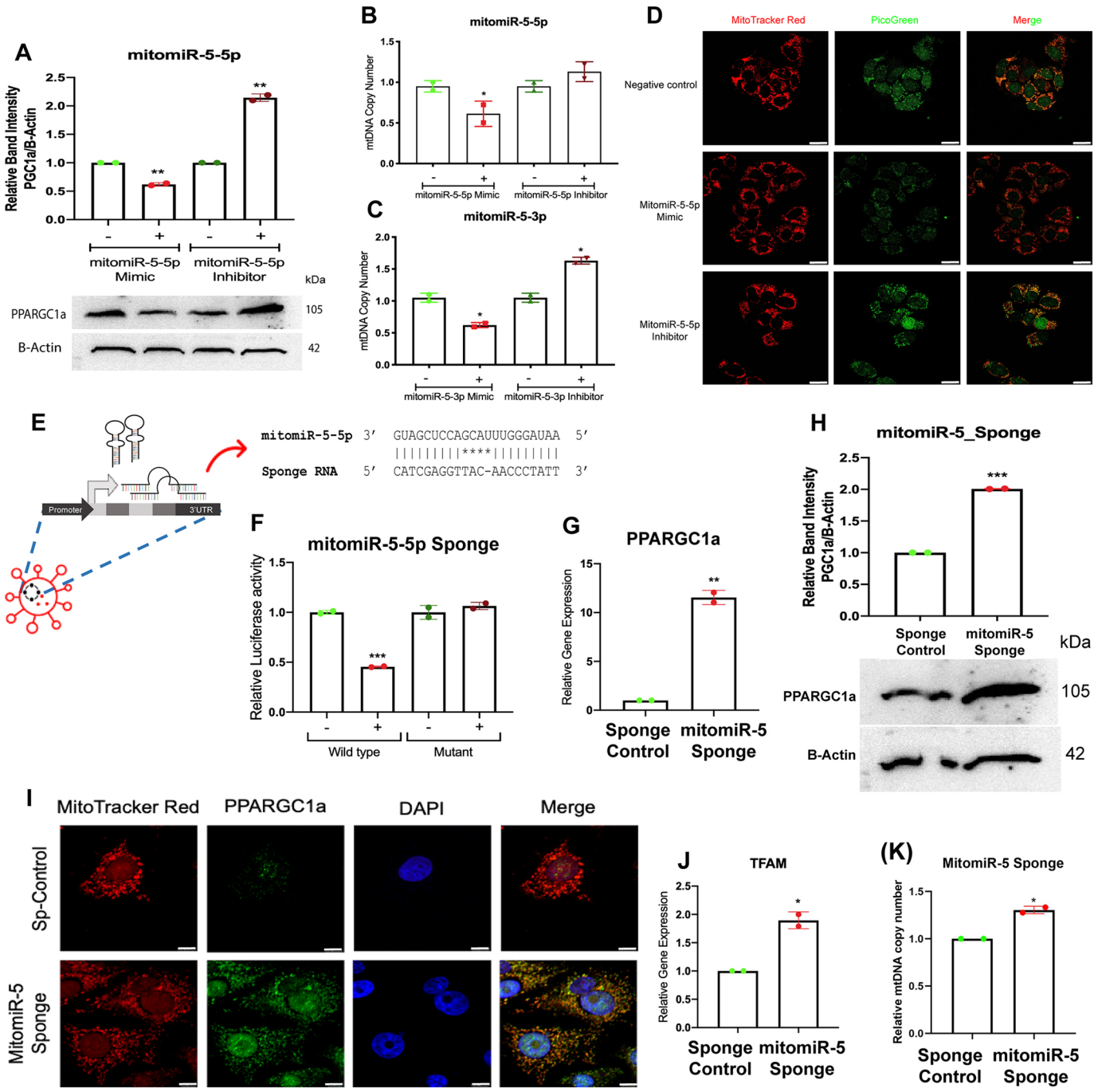

Fig. 6. See next page for legend.

mimic-transfected negative control cells (Fig. 6D). Further, we developed a retrovirus-based mitomiR-5 sponge system stably generating mitomiR-5 antisense sequence in breast cancer cell lines (Fig. 6E). Our mitomiR-5 sponges bind to mitomiR-5-5p and inhibit miRNA–mRNA interaction (Fig. 6E). The mitomiR-5 sponge competitively binds to endogenous mitomiR-5 levels and prevents them from interacting with their target genes. This direct interaction was confirmed by the luciferase reporter assay, by cloning designed sponge sequence into pmirGLO vector, suggesting the specificity of the constructed sponge (Fig. 6F). Retrovirus-mediated overexpression of the mitomiR-5 antisense sequence significantly enhanced endogenous PPARGC1α expression at both the RNA and protein level (Fig. 6G,H). Further, immunofluorescence analysis in sponge cells confirmed the upregulation of PPARGC1α in mitomiR-5-5p sponge-transfected cells when compared with sponge control cells (Fig. 6I). PPARGC1α is known to regulate mitochondria biogenesis by regulating NRF1/2, which in turn maintains TFAM expression. TFAM is a known regulator of mitochondrial DNA structure and copy number (Virbasius and Scarpulla, 1994). We found that mitomiR-5 sponge-transfected cells showed a marked increase in TFAM expression when compared with sponge control cells (Fig. 6J). Subsequently, we observed that along with PPARGC1α and TFAM overexpression, there is an increase in mtDNA copy number in mitomiR-5 sponge-transfected cells when compared with sponge control cells (Fig. 6K).

Journal of Cell Science (2022) 135, jcs258937. doi:10.1242/jcs.258937

Fig. 6. Expression of mitomiR-5-5p regulates mtDNA content in breast cancer cells. (A) Western blot results showing that mitomiR-5-5p regulates endogenous PPARGC1α protein levels in MCF-7 cell line at 48 h transfection with 75 nM mimic and inhibitor along with the respective control oligonucleotides. Densitometric analysis was performed upon normalization of PPARGC1α protein band intensity to the respective β-actin band. Negative sign in the images represent the scrambled mimic control and scrambled inhibitor control oligonucleotides, for all the mimic and inhibitor transfected experiments. *n*=3. (B,C) MitomiR-5-5p (B) and mitomiR-5-3p (C) mimic-transfected cells showed decreased mtDNA copy number, whereas inhibitor-transfected cells show increase in the levels of mtDNA copy number. qRT-PCR was performed after 48 h of transfection with mitomiR-5-5p and mitomiR-5-3p mimic and inhibitor along with control oligonucleotides. Relative quantity was calculated using the formula $2^{-\Delta\Delta C_T}$ to plot the fold change of mtDNA copy number in comparison to the respective control oligonucleotides. The negative signs in the images represent the scrambled mimic control or scrambled inhibitor control oligonucleotides, for all the mimic and inhibitor transfected experiments. *n*=3. (D) MitomiR-5-5p mimic-transfected cells with increased mitomiR-5-5p expression showed decreased mtDNA content when compared with scrambled mimic control. Inhibition of mitomiR-5-5p activity by using mitomiR-5-5p specific inhibitor restores mtDNA content in the mitomiR inhibitor-transfected cells. PicoGreen (green) stains nuclear and mitochondrial DNA and MitoTracker Red (red) stains mitochondria. Live images were acquired with a 63× oil immersion objective of a confocal fluorescent microscope. Images are representative of three independent experiments. Scale bar: 25 µm. (E) Diagrammatic representation of mitomiR-5 sponge generation strategy, as explained in the Materials and Methods section. (F) Luciferase reporter assay showing the specificity of mitomiR-5 sponge to the endogenous mitomiR-5. pmirGLO-cloned mitomiR-5 sponge sequence or mutant constructs were co-transfected with 50 nM of mitomiR-5-5p mimics in MCF-7 cells. Luciferase assay was performed after 24 h of transfection and luciferase activity was normalized to *Renilla* luciferase to calculate relative change. *n*=3. (G) MitomiR-5 sponge over-expressing cells showed increased *PPARGC1A* expression when compared to sponge control cells. *n*=3. (H) Western blot analysis of PPARGC1α protein expression in control and mitomiR-5 sponge cell lines. Densitometric analysis was performed upon normalization of PPARGC1α protein band intensity to respective β-actin band. *n*=3. (I) Immunofluorescence imaging of PPARGC1α stained with Alexa Fluor 488 in control and sponge cells co-stained with MitoTracker Red and DAPI. Images were acquired using a100× oil immersion objective of a confocal fluorescent microscope. Images are representative of three independent experiments. Scale bar: 10 µm. (J) *TFAM*, a downstream target of *PPARGC1A* and transcription factor for mtDNA, was upregulated in mitomiR-5 sponge transfected cells. *n*=3. (K) Increased levels of mtDNA copy number observed in mitomiR-5 sponge cells compared to sponge control cells. Relative quantity was calculated using the formula $2^{-\Delta\Delta C_T}$. *n*=3. **P*<0.05, ***P*<0.001 and ****P*<0.0001 (paired two-tailed Student's *t*-test).

DISCUSSION

Mitochondria are semi-autonomous organelles, known to harbor various regulatory non-coding RNAs and proteins encoded by the nuclear genome for their functioning (Liu et al., 2013; Mercer et al., 2011). The shuttling of RNAs and proteins between the cytoplasm and mitochondria plays a major role in anterograde and retrograde signaling (Vendramin et al., 2017). Critical insights into possible mitomiRs encoded by the mitochondrial genomes is an emerging field of research (Bandiera et al., 2013; Borralho et al., 2015). Recently, there has been a growing interest in identifying mitochondrial genome-encoded non-coding RNAs and their roles in regulating mitochondrial functions (Fitzpatrick et al., 2019). Mitochondrial genome-encoded miRNAs have been predicted by whole mitochondrial transcriptome analysis (Mercer et al., 2011; Ro et al., 2013; Shinde and Bhadra, 2015). Other mitochondrial deep sequencing and small RNA sequencing studies report lncRNA and mitosRNA in humans (Rackham et al., 2011). In this study, we identified pre-mitomiRs that are encoded by mtDNA and predicted their target genes using bioinformatic analysis. Analysis of small RNA sequencing data showed that heavy (H) strand-specific reads primarily come from the sense strand whereas the majority of the light (L) strand-specific reads come from the antisense strand. Analysis of our predicted mitomiRs compared with the previously published non-coding RNAs from mitochondria showed sequence similarity between pre-mitomiR-4 with miR-4485 and miR-1973. This could be possible as miR-4485 and miR-1973 originate from the nuclear mitochondrial pseudogene *MTRNR2L8* (Fig. S8). Our analysis of mitomiR expression data in breast cancer cell lines that are available in public databases showed differential expression levels in different subtypes of breast cancer. Our study confirmed the presence of mitomiR expression using previously published mitochondrial transcriptome datasets by Mercer et al. (2011). Subsequently, mitomiR expression analysis by small RNA sequencing and validation by qRT-PCR in breast cancer cell lines showed their differential expression in a subtype-specific manner, suggesting functional roles for mitomiRs in breast cancer mitochondria. Among the mitomiRs, mitomiR-5 showed significantly higher expression in all three breast cancer cell lines. The stem-loop reverse transcription-based strategy employed in the quantification of selected mitomiRs, confirmed the specificity of the quantified microRNAs (Chen, 2005). Interestingly, mitomiR-5 was differentially expressed in other cancer cell lines. This could possibly be due to the heterogeneity of mitochondrial profiles in these cell lines of different tissue origins, indicating a possible role of mitomiR-5 in tissue-specific gene regulation. MitomiR-5 was significantly expressed in tumor tissue specimens when compared with adjacent normal tissue in the matched breast tumor specimens. Increased mitomiR-5 expression was observed in a small patient cohort of grade 1 tumors when compared with grade 3 tumors, suggesting that mitomiRs expression may be associated with the early stages of breast cancer development. However, more detailed studies in clinical specimens from breast cancer patient cohorts are needed before further conclusions can be drawn.

Low concentrations of ethidium bromide inhibit mitochondrial transcription without altering the mtDNA copy number (Surovtseva and Shadel, 2013), whereas DDC inhibits the replication of mtDNA by acting as a cytidine analogue, thereby terminating the replication chain and competitive occupation of the nucleotide-binding site of POLG (Brown and Clayton, 2002). We found that inhibition of both mtDNA transcription by EtBr exposure and mtDNA replication by DDC significantly reduced mtDNA-encoded *MT-CO2* transcript levels and mitomiR expression, suggesting that mitomiRs are encoded by the mitochondrial genome. Similarly, the knockdown of TFAM led to decreased mitochondrial transcription and mtDNA content in MDA-MB-231 cells. Expression analysis of mitomiRs in TFAM KD cells showed significantly downregulated mitomiR-5-5p expression levels, confirming that the mitochondrial transcription machinery is crucial for mitomiR expression. Interestingly, mitomiR-5 expression was downregulated when breast cancer cells were treated with the known mitochondrial respiratory chain inhibitor antimycin A (complex III). This could be due to perturbed mtDNA replication and transcription as antimycin A is a known inducer of mitochondrial ROS and mtDNA damage (Sarmiento-Salinas et al., 2019). Tetracycline is a well-known translation inhibitor of mitochondria, induces proteotoxic stress and mitonuclear protein imbalance in mitochondria (Moullan et al., 2015). Sub-lethal doses of tetracycline reduced mitomiR-5 levels, suggesting the possibility that nuclear-encoded mitochondrial proteins function in the biogenesis of mitomiRs.

Previously, among the RISC proteins, only Ago2 protein has been identified inside mitochondria. Western blot analyses have shown the absence of GW182 (glycine-tryptophan protein of 182 kDa)

Journal of Cell Science (2022) 135, jcs258937. doi:10.1242/jcs.258937

inside mitochondria, which is important for miRNA gene repression in the cytoplasm (Bandiera et al., 2011; Zhang et al., 2014). We found that mitomiR-5 is associated with Ago2 in both mitochondrial and cytoplasmic fractions. Immunofluorescence analysis using a biotinylated mitomiR-5 mimic showed that mitomiRs are predominantly localized inside mitochondria. qRT-PCR analysis of Ago2 IP elutes showed physical interaction of mitomiR-5 with Ago2, along with PPARGC1α in the cytoplasmic fraction and the mitochondrial transcripts *MT-CO1* and *MT-CO2* in the mitochondrial fraction. Ago2 IP in TFAM KD cells suggested the direct effect of mitomiR-5 downregulation on the interaction between Ago2 and mitomiR-5. These data suggest that mitomiRs are encoded in mitochondria and possibly transported outside the mitochondria for their function. It has been reported that Ago2 co-imports nuclear miRNAs inside mitochondria (Srinivasan and Das, 2015). Another study has shown that the mitochondrial genome encodes ncRNAs localized to the nucleus (Landerer et al., 2011). However, the mechanism of mitomiRs transport from mitochondria to the cytoplasm is yet to be fully understood. Similarly, there are reports of mitomiRs directly regulating mitochondrial gene expression by targeting mtDNA encoded transcripts (Fan et al., 2019; Sripada et al., 2017; Zhang et al., 2014). MitomiR-5-5p directly targets PPARGC1α and reduced its expression in mimic-transfected MDA-MB-468 cells, which was reversed by the mitomiR-5-5p inhibitor. *PPARGC1A* is an essential gene that coordinates mitochondrial biogenesis (Gleyzer et al., 2005; LeBleu et al., 2014). Increased mitomiR-5 expression in mimic-transfected cells showed decreased PPARGC1α expression and subsequent decrease in mtDNA copy number, suggesting that mitomiRs may play a role in regulating mitochondrial biogenesis. Conversely, sponging mitomiR-5 with antisense mitomiR-5-expressing retroviral constructs upregulated PPARGC1α levels in breast cancer cells at the transcript and protein levels. *PPARGC1A* regulates mtDNA transcription by increasing the expression of its downstream target TFAM (Kelly and Scarpulla, 2004). We observed that along with PPARGC1α and TFAM overexpression, there is an increase in mtDNA copy number in mitomiR-5 sponge-transfected cells. *PPARGC1A* is known to promote metabolism, survival, and therapy resistance in breast cancer (Andrzejewski et al., 2017; LeBleu et al., 2014). Targeting mitochondrial biogenesis using mitomiRs could be explored for preclinical studies in therapy-refractory breast cancer patients. Interestingly, mitomiR-5 mimic-transfected cells showed increased *MT-CO1* and *MT-CO2* expression at the transcript level and a subsequent increase in MT-CO2 protein expression along with a moderate increase in complex IV enzyme activity in TNBC cells. Earlier, miR-1 was reported to directly target *MT-CO1* and *MT-ND1* during skeletal muscle biogenesis to enhance mitochondrial translation (Zhang et al., 2014). This phenomenon was supported by the absence of GW182 proteins in the mitochondria, where GW182 proteins are known to recruit some of the decapping and deadenylating enzymes that can destabilize the target mRNAs (Zhang et al., 2014).

The mechanism of mitochondrial miRNA biogenesis and processing is an area that remains to be explored. miRNAs originating from the intronic regions of the genome, known as mirtrons, bypass Drosha-mediated processing by splicing and yield Dicer substrates (Ruby et al., 2007). There are also reports on Dicer-independent miRNA biogenesis where pre-miRNA miR-451 was reported to have directly loaded into the RISC complex and processed by Ago proteins to form an intermediate 3′ end (Cheloufi et al., 2010). These reports suggest such possible non-canonical pathways for mitomiRs biogenesis inside mitochondria.

The role of mitochondrial genome-encoded miRNAs is an attractive yet challenging area of research. More mechanistic data needs to be generated to elucidate the mechanisms of mitomiR biogenesis, transport to the cytoplasm and interacting partners in the mitochondrial RISC complex.

MATERIALS AND METHODS

Cell lines, reagents, and antibodies

Breast cancer cell lines MCF-7 (luminal A), MDA-MB-468 (triple-negative breast cancer, claudin high), MDA-MB-231 (triple-negative breast cancer, claudin low), IMR-32 and SHSY-5Y (neuroblastoma) were cultured in Dulbecco's Modified Eagle Medium/Nutrient Mixture F-12 (DMEM/F12; HiMedia, India) supplemented with 10% fetal bovine serum (FBS) (Gibco, USA). Non-malignant human mammary epithelial cell lines MCF-10A were cultured in DMEM/F12 supplemented with 5% horse serum (Gibco, USA), insulin (Sigma, USA), hydrocortisone (Sigma, USA) and epidermal growth factor protein (Gibco, USA) as per the standard media recommendations from American Type Culture Collection (ATCC, USA). The cancer cell lines SiHa, HeLa and CaSki (cervical cancer), PC3 (prostate cancer), HepG2 (hepatocellular cancer), A549 (lung cancer) and THP1 (leukemia), non-cancer cell line HEK293, and primary cells such as peripheral blood mononuclear cells (PBMCs) and foreskin fibroblasts were cultured in DMEM (HiMedia, India) with 10% FBS. All the cell lines were procured from the ATCC and were grown at 37°C in a humidified chamber with 5% CO_2. All the cell lines were authenticated using STR profiling.

2′,3′-dideoxycytidine, ethidium bromide, sodium pyruvate, uridine, nonidet-P40, cytochrome c oxidase, digitonin, Bradford reagent, Nonyl Acridine Orange, and sodium azide were purchased from Sigma, USA. Protease inhibitor cocktail was purchased from Roche, Switzerland; Nitrocellulose membrane and ECL reagents were bought from Bio-Rad, USA.

For western blot analysis, the primary antibodies used in the study were: anti-Ago2 rabbit monoclonal antibody (mAb) (C34C6), anti-COXIV rabbit mAb (3E11), anti-TFAM rabbit polyclonal antibody (#7495), anti-GAPDH rabbit mAb (14C10) and anti-β-actin rabbit mAb (#4967), procured from Cell Signaling Technology; anti-MT-CO2 mAb (12C4F12), anti-PPARGC1α rabbit polyclonal antibody (PA5-72948) and anti-myc-tag mouse mAb (Myc.A7), procured from Invitrogen, USA. All the primary antibodies were used at a 1:2500 dilution, except for GAPDH and β-actin, which were used at a 1:5000 dilution. HRP-conjugated secondary antibodies, IgG anti-rabbit and IgG anti-mouse were procured from Cell Signaling Technologies and used at a 1:5000 dilution.

Breast cancer patient specimens

Human breast cancer tissue specimens were obtained from patients undergoing biopsy with written consent after approval by Kasturba Medical College and Institutional Ethics Committee (IEC), Kasturba Hospital, Manipal, India (IEC11/2016). Patient clinicopathological details are listed in Table S4. Both tumor and normal tissues (5 cm away from the tumor) were collected from the same patient, transferred to RNA*later* (Invitrogen, USA), and stored at −80°C, until RNA extraction. Clinical investigation was conducted according to the principles expressed in the Declaration of Helsinki. Total RNA was isolated from both tissue specimens and cell lines using the *mir*Vana™ miRNA isolation kit (Invitrogen, USA) and Trizol (Invitrogen, USA), respectively, according to the manufacturer's instructions.

Bioinformatics analysis

In silico predictions of mitomiRs were performed using the revised Cambridge reference sequence (rCRS) of human mitochondrial DNA (Accession: NC_012920; gi:251831106) with an *ab initio* method by miRNAFold (Tempel and Tahi, 2012). Thermodynamic properties and formation of the secondary structure of selected precursor sequences were analyzed using Vienna RNA Websuite (RNAfold) (Gruber et al., 2008) and miREval 2.0 (Gao et al., 2013), respectively. The short-listed mitomiR precursor sequences were used to predict the mature miRNA sequences using MatureBayes (Gkirtzou et al., 2010). Multiple sequence alignment (MSA) was performed in ClustalW (Thompson et al., 2003) and visualized in

MEGA7.0 (Kumar et al., 2016). *In silico* target gene prediction was performed using the multiple target gene prediction tools miRDB (Wang, 2008), Diana MR-microT (Reczko et al., 2012), RNAhybrid (Rehmsmeier et al., 2004), miRanda algorithm (Enright et al., 2003) and RNA22 (Miranda et al., 2006). The top 20 target genes were selected from each tool, and genes that were common in at least two target prediction algorithms were shortlisted for experimental validation. Fig. 1A describes the scheme for *in silico* analysis and prediction of miRNAs encoded by mitochondrial genome (mitomiRs).

Expression analysis of mitomiRs using public databases

Small RNA sequencing analysis using the public datasets European Nucleotide Archive (ENA; project accession ID: PRJNA640820; various subtypes of breast cancer cell lines), Gene Expression Omnibus (Accession IDs: GSE30772 and GSE26328; pure mitochondria and mitoplast datasets of 143B cell lines) and RNA atlas datasets such as neuroblastoma, central nervous system (CNS) cell lines and normal brain tissue samples consisting of various tissue types of brain (Lorenzi et al., 2021) (ENA ID: PRJNA576920) were used for mitomiR expression analysis. FastQ files were downloaded (Leinonen et al., 2011), quality checked with FastQC algorithm and aligned using RNA-STAR that aligns non-contiguous sequences (Dobin et al., 2013) directly onto the reference genome, human hg38 GTF. Finally, the reads were mapped and extracted using SHRiMP v2.2.3 (David et al., 2011).

Small RNA sequencing

Small RNA sequencing was performed in total RNA isolated from MCF-10A, MCF-7 and MDA-MB-468 cell lines. Quality and quantity of the isolated RNA were assessed using agarose gel electrophoresis, RNA 6000 chip using Bioanalyzer 2000 instrument (Agilent Tech, USA) and Qubit™ RNA HS quantification kit (ThermoFisher, USA), respectively. Small RNA enrichment and sample barcoding were performed using Total RNA-Seq Kit V2 followed by library construction and amplification using Ion OneTouch™ 2 System (ThermoFisher, USA) after quality and quantity assessment. Small RNA sequencing was performed using the Ion PGM™ platform. The protocols were followed according to the manufacturer's instructions. Small RNA sequencing data was analyzed for quality control and pre-processing to filter out low-quality reads. The pre-processing was performed using FASTX-toolkit by trimming the reads within 17–35 bases having a quality score above 20. Pre-processed reads were aligned to the predicted 13 mitomiR precursor sequences using SHRiMP v2.2.3 (David et al., 2011), which exclusively aligns short reads with high accuracy. Pre-processed reads were also aligned to the human genome (assembly GRCh38) to isolate nuclear and mitochondrial genome reads. Differential miRNA expression was calculated using DESeq2 (Love et al., 2014) Bioconductor package in R statistical environment.

Pure mitochondria isolation

Crude mitochondria were isolated as per the previously published protocol (Spinazzi et al., 2012) with minor modifications for obtaining pure mitochondria. Briefly, cells were washed with ice-cold PBS, lysed with hypotonic tris-HCl in a PYREX® Potter-Elvehjem homogenizer and subjected to differential centrifugation. After the crude mitochondrial pellets were washed thrice in wash buffer, they were subjected to RNase A (Sigma, USA) treatment to get a pure mitochondrial fraction devoid of cytoplasmic RNA contaminants. Mitoplasts were prepared from pure mitochondrial fractions as reported earlier (Greenawalt, 1974). Both mitochondria and mitoplasts were confirmed for their purity in RNA and protein content by reverse transcription PCR (Fig. S1) and western blotting analysis (Fig. 4B), respectively.

cDNA conversion and real-time PCR

Both miRNA specific cDNA and total cDNA conversion was performed from the RNA isolated from breast cancer cell lines and tissue specimens using TaqMan MicroRNA Reverse Transcription kit and High-Capacity cDNA Reverse Transcription kit (Applied Biosystems, USA), respectively. Real-time PCR was performed for mitomiR expression analysis using custom miRNA TaqMan assays (Applied Biosystems, USA) and gene expression analysis using PowerUp SYBR Green Master Mix (Applied Biosystems, USA). The gene expression primers used in the study are listed in Table S5. Custom microRNA TaqMan assays were designed to perform reverse transcription of novel microRNA sequences on to stem-loop back bone to increase the sensitivity and specificity of the microRNA quantification (Chen, 2005). For mitochondrial DNA copy number analysis, TaqMan gene expression assay *MT-ND1* (test gene) and TaqMan copy number reference assay *RNase P* (reference gene) were used. MitomiRs expression were normalized using endogenous control 5S rRNA (for mitochondrial fraction RNA) and RNU6B (for total RNA from cell lines and tissue samples). Relative quantity (RQ) was calculated using the formula $2^{-\Delta\Delta C_T}$ for all the expression analysis in cell lines, whereas the RQ for tissue samples was calculated with the formula $2^{-\Delta\Delta C_T}$. For mitomiRs expression analysis in clinical specimens, luminal A (n=20), triple-negative (n=20) and Her2-positive (n=20) breast cancer clinical tissue specimens with matched normal controls of each were utilized in the present study.

EtBr, DDC and mitochondrial inhibitors treatment

MCF-7 cell lines were treated with EtBr (50 ng/ml) for 3 and 6 h and DDC (2 µM) for a passage, supplemented with sodium pyruvate (100 µg/ml), uridine (50 µg/ml) and glucose (4.5 mg/ml) in the corresponding media (Nelson et al., 1997; Surovtseva and Shadel, 2013). After the treatment, DNA and total RNA were isolated from an equal number of both EtBr- and DDC-treated cells. Isolated DNA was used for mitochondrial DNA copy number, total RNA was used for gene expression analysis of *MT-CO2* and *ACTB* along with mitomiR-5-5p, mitomiR-5-3 and miR-200b expression using qRT-PCR. Mitochondrial inhibitor antimycin A (25 nM and 100 nM) and tetracycline (1 µM) (Moullan et al., 2015) were used to treat MCF-7 cells for 24 h, and the expression of mitomiR-5-5p, mitomiR-5-3p and miR-146a was analyzed using qRT-PCR.

TFAM knockdown cell lines

TFAM KD (siTFAM) cells were generated using a piLenti-siRNA-GFP lentiviral plasmid (ABMgood, Canada) in MDA-MB-231 cells. Packaging, envelop and transfer plasmids were transfected using Lipofectamine 3000 (Applied Biosystems, USA) according to the manufacturer's instructions along with scrambled siRNA GFP control plasmid. Viral titers from HEK293T cells were transduced into MDA-MB-231 cells after 48 and 72 h. TFAM KD clones were selected after puromycin (2 µg/ml) treatment. Clones were confirmed for TFAM KD using immunoblotting along with scrambled controls.

Plasmid constructs

Plasmid constructs used in the study were generated as per standard cloning techniques. For target gene validation, target gene regions with mitomiR-5 binding sites were cloned into pmirGLO-miRNA target expression vector (Promega, USA). Mutant constructs for target gene validation were generated by Q5 site-directed mutagenesis kit (NEB, USA). Ago2 full length CDS region was cloned into pCMV/myc/mito plasmid, which was deposited by David Sidransky (Addgene plasmid #71542; RRID: Addgene_71542) (Dasgupta et al., 2008), to generate MCF-7 cells stably expressing Ago2 protein in the mitochondrial compartment. Briefly, the respective inserts were PCR amplified, restriction digested and gel eluted, along with empty vectors. Purified inserts and vectors with respective sticky ends were ligated using T4 DNA ligase (NEB, USA), followed by transformation into DH10β chemical competent cells using the standard heat shock method. Plasmids were isolated, and insert sequences were confirmed with restriction digestion and Sanger DNA sequencing prior to downstream applications. The cloning primers used in the study are listed in Table S6.

To create the stable sponge model, we designed antisense mitomiR-5 sponge oligonucleotides to clone into the retroviral expression vector pMSCV-PIG (Puro IRES GFP empty vector), which was deposited by David Bartel (Addgene plasmid #21654; RRID: Addgene_21654) (Mayr and Bartel, 2009), as described previously (Kluiver et al., 2012). Briefly, sense and antisense sequences of both linker and sponge sequences were 5′-

phosphorylated and mixed in equimolar concentration. This mixture was heated in boiling water for 10 min and cooled to room temperature slowly for 30 min to generate oligonucleotide duplex. The duplex was then cloned into the target vector using T4 DNA ligase at a 1:300 ratio. Linker sequence was first cloned to introduce a Kfl1/SanD1 site into the plasmid between Xho1 and EcoR1 sites. MitomiR-5-5p sponge oligonucleotides were designed with Kfl1/SanD1 sticky ends on both the sides to facilitate directional cloning into linker sequence-cloned pMSCV vector. After digestion with the Kfl1/SanD1 enzyme, mitomiR-5-5p sponge duplex was cloned similar to linker cloning. Finally, the clones were verified by PCR amplification using plasmid-specific primers and Sanger DNA sequencing. Clones with maximum copy sponge plasmid were transduced into MCF-7 breast cancer cell lines and selected using 1 µg/ml of puromycin. MitomiR-5 sponge sequences were also cloned into the pmirGLO vector to validate the specificity of mitomiR-5 sponge sequences to the endogenous mitomiR-5 using luciferase reporter assay.

Target gene validation

Wild-type and mutant constructs of *in silico*-predicted target genes cloned into pmirGLO plasmids were co-transfected with 50 nM of mitomiR-5 mimic and scrambled negative control oligonucleotides (Invitrogen, USA) into MCF-7 cell lines using Lipofectamine 3000 reagent. Luciferase assay was performed using Dual-Luciferase Reporter assay kit (Promega, USA) using *Renilla* luciferase as an internal control after 24 h of transfection. Target gene validation was also confirmed by qRT-PCR-based expression analysis and immunoblotting in the MDA-MB-468 cell line. Mitochondrial complex IV enzyme activity assays, mitochondrial DNA (mtDNA) copy number assays and mitochondrial mass analyses were performed to study the impact of mitomiR expression on mitochondrial function.

Western blot analysis

Cells were lysed using RIPA buffer supplemented with protease inhibitor cocktail to extract total proteins from the respective cell lines and protein quantification was performed using Bradford assay. Briefly, lysed cells were resolved on 10–12% SDS-PAGE gels, transferred onto nitrocellulose membranes, blocked using 5% BSA or non-fat dry milk and incubated separately with respective primary antibodies at 4°C overnight. Following primary antibody incubation, the blots were developed with the respective HRP-conjugated secondary antibodies for 1 h at room temperature. Finally, bands were visualized using ECL reagent in ImageQuant LAS 4000 system (GE Healthcare). All the protein bands were normalized to the loading control β-actin upon densitometric analysis performed using ImageJ (Fiji software). Raw data of the western blot images are provided in Figs S9–S13.

Ago2 IP

Ago2 IP was performed using the mitochondrial protein immunoprecipitation kit (Sigma, USA) according to the manufacturer's instructions. Briefly, the pure mitoplast fraction or whole cell lysate fractions were lysed in lysis buffer containing Nonidet P-40 and the supernatants were collected after centrifugation. These lysates were incubated with Ago2 rabbit mAb or Myc-tag mouse mAb at a 1:50 dilution along with equal concentrations of rabbit or mouse IgG antibodies at 4°C overnight on a nutator mixer. The protein–antibody immunocomplex was then separated using 1.5 mg of Protein A Dynabeads (Life Technologies, USA) on a magnetic stand. The beads were thoroughly washed with wash buffer containing Tween-20, and RNA was isolated with Trizol reagent for mitomiR and target gene expression.

Imaging for mitochondrial morphology, mitomiR-5 localization and mtDNA

For live imaging analysis, MCF-7 cells transfected with mitomiR-5 mimic and inhibitor oligonucleotides were grown on sterile coverslips for 48 h, washed with PBS and incubated with serum-free media containing 100 nM MitoTracker™ Red CMXRos and Quant-iT™ PicoGreen™ dsDNA Reagent (Life Technologies, USA) as per the manufacturer's instructions. After 20 min of incubation in the dark at 37°C, cells were washed with PBS and imaged in Phenol Red-free media for live imaging. For mitomiR localization studies, custom mitomiR-5-5p mimic sequences (Dharmacon, USA) were designed with a 5′ Biotin tag. After 24 h of transfection with 75 nM biotinylated mimic or scrambled negative control oligonucleotides, the cells were processed according to fixed imaging protocol. For fixed imaging analysis, cells grown on sterile coverslips were stained with 300 nM MitoTracker Red, fixed with 4% paraformaldehyde for 15 min at 37°C, permeabilized with 0.1% Tween-20, followed by blocking with 5% FBS at room temperature. Subsequently, the cells were incubated in 4°C with the respective primary antibodies overnight and secondary antibodies for 2 h at room temperature. For mitomiR-5-5p localization analysis, coverslips from the blocking step were directly subjected to streptavidin Alexa Fluor 488 (Invitrogen, USA) staining for 1 h. Subsequently, nuclear staining was performed with DAPI (Sigma, USA) and mounted with Mowiol and stored at 4°C in the dark. Mitochondrial DNA content, mitomiR-5 localization as well as mitochondrial morphology were assessed using Leica TCS SP8 platform with DMi8 confocal microscope along with LAS X software (Leica Microsystems, Germany).

Fluorescence-activated cell sorting analysis for mitochondria mass

2×10^5 cells intended for mitochondria mass analysis were seeded on 6 cm Petri plates. Cells were stained with Nonyl Acridine Orange (NAO) in serum-free media at a final concentration of 10 µM for 30 min at 37°C. After the staining, cells were trypsinized, washed with PBS and used for fluorescence-activated cell sorting (FACS) analysis (Partec, Germany).

Mitochondrial complex IV activity assay

Mitochondrial complex IV activity assay was performed as reported earlier (Spinazzi et al., 2012). Briefly, base line absorbance of reduced cytochrome c oxidase was measured in phosphate buffer. Subsequently, the enzyme activity of cytochrome c oxidase from 10^5 cells was measured at 550 nm using a Varioskan Flash microplate reader (Thermo Scientific, USA). Complex IV specific inhibitor sodium azide was used to calculate the specific activity with the formula: enzyme activity (nmol/min/mg)=(Change in Absorbance/min×1000)/[(reduced cytochrome c oxidase extinction coefficient×volume of the sample lysate used in ml)×(sample protein concentration in mg/ml)].

Statistical analysis

Statistical analyses were performed using GraphPad Prism 8.0 (La Jolla, CA). Paired two-tailed Student's *t*-tests were performed for all the two group comparison experiments, whereas two-way ANOVA with Tukey's honestly significant difference (Tukey HSD) post-hoc test were performed for comparisons between more than two groups. $P<0.05$ was considered statistically significant.

Acknowledgements

We are grateful to the patients for their participation.

Competing interests

The authors declare no competing or financial interests.

Author contributions

Conceptualization: S.C.; Methodology: R.K., S.C.; Software: R.K., V.S., S.M., D.A., S.C.; Validation: R.K., S.C.; Formal analysis: R.K., S.C.; Investigation: R.K., S.C.; Resources: R.K., L.R., P.U.P.S.; Data curation: R.K., V.S., S.M., D.A., L.R., S.C.; Writing - original draft: R.K., S.C.; Writing - review & editing: S.P.K., K.S., S.C.; Visualization: R.K., S.C.; Supervision: S.C.; Project administration: S.C.; Funding acquisition: S.C.

Funding

This work was supported by Science and Engineering Research Board (SERB) (YSS/2015/001051 and CRG/2020/004681). R.K. was supported by an Indian Council of Medical Research Senior Research Fellowship (ICMR-SRF; File No: 2019-0278/GEN-BMS). Infrastructure support and funding was provided by Department of Science and Technology, Ministry of Science and Technology, India Fund for Improvement of S&T Infrastructure (DST-FIST), Technology Information, Forecasting and Assessment Council (TIFAC) Centre of Relevance and Excellence (CORE), Vision Group on Science and Technology (VGST), Karnataka Fund for Infrastructure Strengthening in Science and Technology (K-FIST) and Manipal Academy of Higher Education.

Peer review history
The peer review history is available online at https://journals.biologists.com/jcs/article-lookup/doi/10.1242/jcs.258937.

References

Ambros, V. (2004). The functions of animal microRNAs. *Nature* **431**, 350-355. doi:10.1038/nature02871

Andrzejewski, S., Klimcakova, E., Johnson, R. M., Tabariès, S., Annis, M. G., McGuirk, S., Northey, J. J., Chénard, V., Sriram, U., Papadopoli, D. J. et al. (2017). PGC-1α promotes breast cancer metastasis and confers bioenergetic flexibility against metabolic drugs. *Cell Metab.* **26**, 778-787.e5. doi:10.1016/j.cmet.2017.09.006

Bandiera, S., Rüberg, S., Girard, M., Cagnard, N., Hanein, S., Chrétien, D., Munnich, A., Lyonnet, S. and Henrion-Caude, A. (2011). Nuclear outsourcing of RNA interference components to human mitochondria. *PLoS One* **6**, e20746. doi:10.1371/journal.pone.0020746

Bandiera, S., Matégot, R., Girard, M., Demongeot, J. and Henrion-Caude, A. (2013). MitomiRs delineating the intracellular localization of microRNAs at mitochondria. *Free Radic. Biol. Med.* **64**, 12-19. doi:10.1016/j.freeradbiomed.2013.06.013

Bianchessi, V., Badi, I., Bertolotti, M., Nigro, P., D'Alessandra, Y., Capogrossi, M. C., Zanobini, M., Pompilio, G., Raucci, A. and Lauri, A. (2015). The mitochondrial lncRNA ASncmtRNA-2 is induced in aging and replicative senescence in Endothelial Cells. *J. Mol. Cell. Cardiol.* **81**, 62-70. doi:10.1016/j.yjmcc.2015.01.012

Bienertova-Vasku, J., Sana, J. and Slaby, O. (2013). The role of microRNAs in mitochondria in cancer. *Cancer Lett.* **336**, 1-7. doi:10.1016/j.canlet.2013.05.001

Borralho, P. M., Rodrigues, C. M. P. and Steer, C. J. (2015). microRNAs in mitochondria: an unexplored niche. *Adv. Exp. Med. Biol.* **887**, 31-51. doi:10.1007/978-3-319-22380-3_3

Brown, T. A. and Clayton, D. A. (2002). Release of replication termination controls mitochondrial DNA copy number after depletion with 2′,3′-dideoxycytidine. *Nucleic Acids Res.* **30**, 2004-2010. doi:10.1093/nar/30.9.2004

Cantó, C., Gerhart-Hines, Z., Feige, J. N., Lagouge, M., Noriega, L., Milne, J. C., Elliott, P. J., Puigserver, P. and Auwerx, J. (2009). AMPK regulates energy expenditure by modulating NAD+ metabolism and SIRT1 activity. *Nature* **458**, 1056-1060. doi:10.1038/nature07813

Chang, H.-C. and Guarente, L. (2014). SIRT1 and other sirtuins in metabolism. *Trends Endocrinol. Metab.* **25**, 138-145. doi:10.1016/j.tem.2013.12.001

Cheloufi, S., Dos Santos, C. O., Chong, M. M. and Hannon, G. J. (2010). A dicer-independent miRNA biogenesis pathway that requires ago catalysis. *Nature* **465**, 584-589. doi:10.1038/nature09092

Chen, C. (2005). Real-time quantification of microRNAs by stem-loop RT-PCR. *Nucleic Acids Res.* **33**, e179. doi:10.1093/nar/gni178

Das, S., Ferlito, M., Kent, O. A., Fox-Talbot, K., Wang, R., Liu, D., Raghavachari, N., Yang, Y., Wheelan, S. J., Murphy, E. et al. (2012). Nuclear miRNA regulates the mitochondrial genome in the heart. *Circ. Res.* **110**, 1596-1603. doi:10.1161/CIRCRESAHA.112.267732

Das, S., Bedja, D., Campbell, N., Dunkerly, B., Chenna, V., Maitra, A. and Steenbergen, C. (2014). miR-181c regulates the mitochondrial genome, bioenergetics, and propensity for heart failure in vivo. *PLoS One* **9**, e96820. doi:10.1371/journal.pone.0096820

Dasgupta, S., Hoque, M. O., Upadhyay, S. and Sidransky, D. (2008). Mitochondrial cytochrome B gene mutation promotes tumor growth in bladder cancer. *Cancer Res.* **68**, 700-706. doi:10.1158/0008-5472.CAN-07-5532

David, M., Dzamba, M., Lister, D., Ilie, L. and Brudno, M. (2011). SHRiMP2: sensitive yet practical short read mapping. *Bioinformatics* **27**, 1011-1012. doi:10.1093/bioinformatics/btr046

Dobin, A., Davis, C. A., Schlesinger, F., Drenkow, J., Zaleski, C., Jha, S., Batut, P., Chaisson, M. and Gingeras, T. R. (2013). STAR: ultrafast universal RNA-seq aligner. *Bioinforma. Oxf. Engl.* **29**, 15-21. doi:10.1093/bioinformatics/bts635

Du, F., Yu, Q., Chen, A., Chen, D. and Yan, S. S. (2018). Astrocytes attenuate mitochondrial dysfunctions in human dopaminergic neurons derived from iPSC. *Stem Cell Rep.* **10**, 366-374. doi:10.1016/j.stemcr.2017.12.021

Enright, A. J., John, B., Gaul, U., Tuschl, T., Sander, C. and Marks, D. S. (2003). MicroRNA targets in Drosophila. *Genome Biol.* **5**, R1. doi:10.1186/gb-2003-5-1-r1

Fan, S., Tian, T., Chen, W., Lv, X., Lei, X., Zhang, H., Sun, S., Cai, L., Pan, G., He, L. et al. (2019). Mitochondrial miRNA determines chemoresistance by reprogramming metabolism and regulating mitochondrial transcription. *Cancer Res.* **79**, 1069-1084. doi:10.1158/0008-5472.CAN-18-2505

Favaro, E., Ramachandran, A., McCormick, R., Gee, H., Blancher, C., Crosby, M., Devlin, C., Blick, C., Buffa, F., Li, J.-L. et al. (2010). MicroRNA-210 regulates mitochondrial free radical response to hypoxia and krebs cycle in cancer cells by targeting iron sulfur cluster protein ISCU. *PLoS One* **5**, e10345. doi:10.1371/journal.pone.0010345

Fitzpatrick, C., Bendek, M. F., Briones, M., Farfan, N., Silva, V. A., Nardocci, G., Montecino, M., Boland, A., Deleuze, J. F., Villegas, J. et al. (2019). Mitochondrial ncRNA targeting induces cell cycle arrest and tumor growth inhibition of MDA-MB-231 breast cancer cells through reduction of key cell cycle progression factors. *Cell Death Dis.* **10**, 423. doi:10.1038/s41419-019-1649-3

Fulco, M., Cen, Y., Zhao, P., Hoffman, E. P., McBurney, M. W., Sauve, A. A. and Sartorelli, V. (2008). Glucose restriction inhibits skeletal myoblast differentiation by activating SIRT1 through AMPK-mediated regulation of Nampt. *Dev. Cell* **14**, 661-673. doi:10.1016/j.devcel.2008.02.004

Gao, D., Middleton, R., Rasko, J. E. J. and Ritchie, W. (2013). MiREval 2.0: a web tool for simple microRNA prediction in genome sequences. *Bioinformatics* **29**, 3225-3226. doi:10.1093/bioinformatics/btt545

Gkirtzou, K., Tsamardinos, I., Tsakalides, P. and Poirazi, P. (2010). MatureBayes: a probabilistic algorithm for identifying the mature miRNA within novel precursors. *PLoS One* **5**, e11843. doi:10.1371/journal.pone.0011843

Gleyzer, N., Vercauteren, K. and Scarpulla, R. C. (2005). Control of mitochondrial transcription specificity factors (TFB1M and TFB2M) by nuclear respiratory factors (NRF-1 and NRF-2) and PGC-1 family coactivators. *Mol. Cell. Biol.* **25**, 1354-1366. doi:10.1128/MCB.25.4.1354-1366.2005

Goud, M. R. and Hua, Z. A. (2015). Role of microRNA in the regulation of mitochondrial functions. *Sci. Lett* **3**, 83-88.

Greenawalt, J. W. (1974). The isolation of outer and inner mitochondrial membranes. *Methods Enzymol.* **31**, 310-323. doi:10.1016/0076-6879(74)31033-6

Gruber, A. R., Lorenz, R., Bernhart, S. H., Neubock, R. and Hofacker, I. L. (2008). The Vienna RNA websuite. *Nucleic Acids Res.* **36**, W70-W74. doi:10.1093/nar/gkn188

Guha, M., Srinivasan, S., Ruthel, G., Kashina, A. K., Carstens, R. P., Mendoza, A., Khanna, C., Van Winkle, T. and Avadhani, N. G. (2014). Mitochondrial retrograde signaling induces epithelial-mesenchymal transition and generates breast cancer stem cells. *Oncogene* **33**, 5238-5250. doi:10.1038/onc.2013.467

Gwinn, D. M., Shackelford, D. B., Egan, D. F., Mihaylova, M. M., Mery, A., Vasquez, D. S., Turk, B. E. and Shaw, R. J. (2008). AMPK phosphorylation of raptor mediates a metabolic checkpoint. *Mol. Cell* **30**, 214-226. doi:10.1016/j.molcel.2008.03.003

Huang, Q., Yan, J. and Agami, R. (2018). Long non-coding RNAs in metastasis. *Cancer Metastasis Rev.* **37**, 75-81. doi:10.1007/s10555-017-9713-x

Kao, L.-P., Ovchinnikov, D. and Wolvetang, E. (2012). The effect of ethidium bromide and chloramphenicol on mitochondrial biogenesis in primary human fibroblasts. *Toxicol. Appl. Pharmacol.* **261**, 42-49. doi:10.1016/j.taap.2012.03.009

Kelly, D. P. and Scarpulla, R. C. (2004). Transcriptional regulatory circuits controlling mitochondrial biogenesis and function. *Genes Dev.* **18**, 357-368. doi:10.1101/gad.1177604

Kluiver, J., Slezak-Prochazka, I., Smigielska-Czepiel, K., Halsema, N., Kroesen, B.-J. and van den Berg, A. (2012). Generation of miRNA sponge constructs. *Methods San Diego Calif* **58**, 113-117. doi:10.1016/j.ymeth.2012.07.019

Kren, B. T., Wong, P. Y.-P., Sarver, A., Zhang, X., Zeng, Y. and Steer, C. J. (2009). MicroRNAs identified in highly purified liver-derived mitochondria may play a role in apoptosis. *RNA Biol.* **6**, 65-72. doi:10.4161/rna.6.1.7534

Kumar, S., Stecher, G. and Tamura, K. (2016). MEGA7: molecular evolutionary genetics analysis version 7.0 for bigger datasets. *Mol. Biol. Evol.* **33**, 1870-1874. doi:10.1093/molbev/msw054

Lan, F., Cacicedo, J. M., Ruderman, N. and Ido, Y. (2008). SIRT1 modulation of the acetylation status, cytosolic localization, and activity of LKB1. Possible role in AMP-activated protein kinase activation. *J. Biol. Chem.* **283**, 27628-27635. doi:10.1074/jbc.M805711200

Landerer, E., Villegas, J., Burzio, V. A., Oliveira, L., Villota, C., Lopez, C., Restovic, F., Martinez, R., Castillo, O. and Burzio, L. O. (2011). Nuclear localization of the mitochondrial ncRNAs in normal and cancer cells. *Cell Oncol. Dordr.* **34**, 297-305. doi:10.1007/s13402-011-0018-8

LeBleu, V. S., O'Connell, J. T., Gonzalez Herrera, K. N., Wikman, H., Pantel, K., Haigis, M. C., de Carvalho, F. M., Damascena, A., Domingos Chinen, L. T., Rocha, R. M. et al. (2014). PGC-1α mediates mitochondrial biogenesis and oxidative phosphorylation in cancer cells to promote metastasis. *Nat. Cell Biol.* **16**, 992-1003. doi:10.1038/ncb3039

Lee, H., Tak, H., Park, S. J., Jo, Y. K., Cho, D. H. and Lee, E. K. (2017). microRNA-200a-3p enhances mitochondrial elongation by targeting mitochondrial fission factor. *BMB Rep.* **50**, 214-219. doi:10.5483/BMBRep.2017.50.4.006

Leinonen, R., Sugawara, H. and Shumway, M., and **International Nucleotide Sequence Database Collaboration** (2011). The sequence read archive. *Nucleic Acids Res.* **39**, D19-D21. doi:10.1093/nar/gkq1019

Leucci, E., Vendramin, R., Spinazzi, M., Laurette, P., Fiers, M., Wouters, J., Radaelli, E., Eyckerman, S., Leonelli, C., Vanderheyden, K. et al. (2016). Melanoma addiction to the long non-coding RNA SAMMSON. *Nature* **531**, 518-522. doi:10.1038/nature17161

Li, J., Donath, S., Li, Y., Qin, D., Prabhakar, B. S. and Li, P. (2010). miR-30 regulates mitochondrial fission through targeting p53 and the dynamin-related protein-1 pathway. *PLoS Genet.* **6**, e1000795. doi:10.1371/journal.pgen.1000795

Li, X., Wang, F. S., Wu, Z. Y., Lin, J. L., Lan, W. B. and Lin, J. H. (2014). MicroRNA-19b targets Mfn1 to inhibit Mfn1-induced apoptosis in osteosarcoma cells. *Neoplasma* **61**, 265-273. doi:10.4149/neo_2014_034

Liu, G., Mercer, T. R., Shearwood, A.-M. J., Siira, S. J., Hibbs, M. E., Mattick, J. S., Rackham, O. and Filipovska, A. (2013). Mapping of mitochondrial RNA-protein interactions by digital RNase footprinting. *Cell Rep.* **5**, 839-848. doi:10.1016/j.celrep.2013.09.036

Long, B., Wang, K., Li, N., Murtaza, I., Xiao, J. Y., Fan, Y. Y., Liu, C. Y., Li, W. H., Cheng, Z. and Li, P. F. (2013). MiR-761 regulates the mitochondrial network by targeting mitochondrial fission factor. *Free Radic. Biol. Med.* **65**, 371-379. doi:10.1016/j.freeradbiomed.2013.07.009

Lorenzi, L., Chiu, H.-S., Avila Cobos, F., Gross, S., Volders, P.-J., Cannoodt, R., Nuytens, J., Vanderheyden, K., Anckaert, J., Lefever, S. et al. (2021). The RNA Atlas expands the catalog of human non-coding RNAs. *Nat. Biotechnol.* **39**, 1453-1465. doi:10.1038/s41587-021-00936-1

Love, M. I., Huber, W. and Anders, S. (2014). Moderated estimation of fold change and dispersion for RNA-seq data with DESeq2. *Genome Biol.* **15**, 550. doi:10.1186/s13059-014-0550-8

Luo, Z., Zang, M. and Guo, W. (2010). AMPK as a metabolic tumor suppressor: control of metabolism and cell growth. *Future Oncol. Lond. Engl.* **6**, 457-470. doi:10.2217/fon.09.174

Marin, T. L., Gongol, B., Zhang, F., Martin, M., Johnson, D. A., Xiao, H., Wang, Y., Subramaniam, S., Chien, S. and Shyy, J. Y.-J. (2017). AMPK promotes mitochondrial biogenesis and function by phosphorylating the epigenetic factors DNMT1, RBBP7, and HAT1. *Sci. Signal.* **10**, eaaf7478. doi:10.1126/scisignal.aaf7478

Mayr, C. and Bartel, D. P. (2009). Widespread shortening of 3'UTRs by alternative cleavage and polyadenylation activates oncogenes in cancer cells. *Cell* **138**, 673-684. doi:10.1016/j.cell.2009.06.016

Mercer, T. R., Neph, S., Dinger, M. E., Crawford, J., Smith, M. A., Shearwood, A. M. J., Haugen, E., Bracken, C. P., Rackham, O., Stamatoyannopoulos, J. A. et al. (2011). The human mitochondrial transcriptome. *Cell* **146**, 645-658. doi:10.1016/j.cell.2011.06.051

Miranda, K. C., Huynh, T., Tay, Y., Ang, Y.-S., Tam, W.-L., Thomson, A. M., Lim, B. and Rigoutsos, I. (2006). A pattern-based method for the identification of MicroRNA binding sites and their corresponding heteroduplexes. *Cell* **126**, 1203-1217. doi:10.1016/j.cell.2006.07.031

Moullan, N., Mouchiroud, L., Wang, X., Ryu, D., Williams, E. G., Mottis, A., Jovaisaite, V., Frochaux, M. V., Quiros, P. M., Deplancke, B. et al. (2015). Tetracyclines disturb mitochondrial function across eukaryotic models: a call for caution in biomedical research. *Cell Rep.* **10**, 1681-1691. doi:10.1016/j.celrep.2015.02.034

Nelson, I., Hanna, M. G., Wood, N. W. and Harding, A. E. (1997). Depletion of mitochondrial DNA by ddC in untransformed human cell lines. *Somat. Cell Mol. Genet.* **23**, 287-290. doi:10.1007/BF02674419

Pelicano, H., Zhang, W., Liu, J., Hammoudi, N., Dai, J., Xu, R.-H., Pusztai, L. and Huang, P. (2014). Mitochondrial dysfunction in some triple-negative breast cancer cell lines: role of mTOR pathway and therapeutic potential. *Breast Cancer Res.* **16**, 434. doi:10.1186/s13058-014-0434-6

Pohjoismäki, J. L. O., Wanrooij, S., Hyvärinen, A. K., Goffart, S., Holt, I. J., Spelbrink, J. N. and Jacobs, H. T. (2006). Alterations to the expression level of mitochondrial transcription factor A, TFAM, modify the mode of mitochondrial DNA replication in cultured human cells. *Nucleic Acids Res.* **34**, 5815-5828. doi:10.1093/nar/gkl703

Rackham, O., Shearwood, A.-M. J., Mercer, T. R., Davies, S. M. K., Mattick, J. S. and Filipovska, A. (2011). Long noncoding RNAs are generated from the mitochondrial genome and regulated by nuclear-encoded proteins. *RNA* **17**, 2085-2093. doi:10.1261/rna.029405.111

Ramachandran, A., Basu, U., Sultana, S., Nandakumar, D. and Patel, S. S. (2017). Human mitochondrial transcription factors TFAM and TFB2M work synergistically in promoter melting during transcription initiation. *Nucleic Acids Res.* **45**, 861-874. doi:10.1093/nar/gkw1157

Reczko, M., Maragkakis, M., Alexiou, P., Grosse, I. and Hatzigeorgiou, A. G. (2012). Functional microRNA targets in protein coding sequences. *Bioinformatics* **28**, 771-776. doi:10.1093/bioinformatics/bts043

Reda, A., Refaat, A., Abd-Rabou, A. A., Mahmoud, A. M., Adel, M., Sabet, S. and Ali, S. S. (2019). Role of mitochondria in rescuing glycolytically inhibited subpopulation of triple negative but not hormone-responsive breast cancer cells. *Sci. Rep.* **9**, 13748. doi:10.1038/s41598-019-50141-z

Rehmsmeier, M., Steffen, P., Höchsmann, M. and Giegerich, R. (2004). Fast and effective prediction of microRNA/target duplexes. *RNA N. Y. N* **10**, 1507-1517. doi:10.1261/rna.5248604

Ro, S., Ma, H.-Y., Park, C., Ortogero, N., Song, R., Hennig, G. W., Zheng, H., Lin, Y.-M., Moro, L., Hsieh, J.-T. et al. (2013). The mitochondrial genome encodes abundant small noncoding RNAs. *Cell Res.* **23**, 759-774. doi:10.1038/cr.2013.37

Ruby, J. G., Jan, C. H. and Bartel, D. P. (2007). Intronic microRNA precursors that bypass Drosha processing. *Nature* **448**, 83-86. doi:10.1038/nature05983

Sarmiento-Salinas, F. L., Delgado-Magallón, A., Montes-Alvarado, J. B., Ramírez-Ramírez, D., Flores-Alonso, J. C., Cortés-Hernández, P., Reyes-Leyva, J., Herrera-Camacho, I., Anaya-Ruiz, M., Pelayo, R. et al. (2019). Breast cancer subtypes present a differential production of reactive oxygen species (ROS) and susceptibility to antioxidant treatment. *Front. Oncol.* **9**, 480. doi:10.3389/fonc.2019.00480

Shen, L., Chen, L., Zhang, S., Du, J., Bai, L., Zhang, Y., Jiang, Y., Li, X., Wang, J. and Zhu, L. (2016). MicroRNA-27b regulates mitochondria biogenesis in myocytes. *PLoS One* **11**, e0148532. doi:10.1371/journal.pone.0148532

Shinde, S. and Bhadra, U. (2015). A complex genome-microRNA interplay in human mitochondria. *Biomed. Res. Int.* **2015**, 206382. doi:10.1155/2015/206382

Spinazzi, M., Casarin, A., Pertegato, V., Salviati, L. and Angelini, C. (2012). Assessment of mitochondrial respiratory chain enzymatic activities on tissues and cultured cells. *Nat. Protoc.* **7**, 1235-1246. doi:10.1038/nprot.2012.058

Srinivasan, H. and Das, S. (2015). Mitochondrial miRNA (MitomiR): a new player in cardiovascular health. *Can. J. Physiol. Pharmacol.* **93**, 855-861. doi:10.1139/cjpp-2014-0500

Sripada, L., Singh, K., Lipatova, A. V., Singh, A., Prajapati, P., Tomar, D., Bhatelia, K., Roy, M., Singh, R., Godbole, M. M. et al. (2017). hsa-miR-4485 regulates mitochondrial functions and inhibits the tumorigenicity of breast cancer cells. *J. Mol. Med.* **95**, 641-651. doi:10.1007/s00109-017-1517-5

Su, Q., Xu, Y., Cai, R., Dai, R., Yang, X., Liu, Y. and Kong, B. (2021). miR-146a inhibits mitochondrial dysfunction and myocardial infarction by targeting cyclophilin D. *Mol. Ther. Nucleic Acids* **23**, 1258-1271. doi:10.1016/j.omtn.2021.01.034

Sun, X., Wang, M., Wang, M., Yu, X., Guo, J., Sun, T., Li, X., Yao, L., Dong, H. and Xu, Y. (2020). Metabolic reprogramming in triple-negative breast cancer. *Front. Oncol.* **10**, 428. doi:10.3389/fonc.2020.00428

Surovtseva, Y. V. and Shadel, G. S. (2013). Transcription-independent role for human mitochondrial RNA polymerase in mitochondrial ribosome biogenesis. *Nucleic Acids Res.* **41**, 2479-2488. doi:10.1093/nar/gks1447

Tak, H., Kim, J., Jayabalan, A. K., Lee, H., Kang, H., Cho, D., Ohn, T., Nam, S. W., Kim, W. and Lee, E. K. (2014). miR-27 regulates mitochondrial networks by directly targeting the mitochondrial fi ssion factor. *Exp. Mol. Med.* **46**, e123. doi:10.1038/emm.2014.73

Tempel, S. and Tahi, F. (2012). A fast *ab-initio* method for predicting miRNA precursors in genomes. *Nucleic Acids Res.* **40**, e80. doi:10.1093/nar/gks146

Thompson, J. D., Gibson, T. J. and Higgins, D. G. (2002). Multiple sequence alignment using ClustalW and ClustalX. *Curr. Protoc. Bioinforma.* Chapter 2, 2.3.1-2.3.22. doi:10.1002/0471250953.bi0203s00

Tomasetti, M., Nocchi, L., Staffolani, S., Manzella, N., Amati, M., Goodwin, J., Kluckova, K., Nguyen, M., Strafella, E., Bajzikova, M. et al. (2014). MicroRNA-126 suppresses mesothelioma malignancy by targeting IRS1 and interfering with the mitochondrial function. *Antioxid. Redox Signal.* **21**, 2109-2125. doi:10.1089/ars.2013.5215

Torregrosa-Muñumer, R., Goffart, S., Haikonen, J. A. and Pohjoismäki, J. L. O. (2015). Low doses of ultraviolet radiation and oxidative damage induce dramatic accumulation of mitochondrial DNA replication intermediates, fork regression, and replication initiation shift. *Mol. Biol. Cell* **26**, 4197-4208. doi:10.1091/mbc.e15-06-0390

Vendramin, R., Marine, J. and Leucci, E. (2017). Non–coding RNAs: the dark side of nuclear–mitochondrial communication. *EMBO J.* **36**, 1123-1133. doi:10.15252/embj.201695546

Vendramin, R., Verheyden, Y., Ishikawa, H., Goedert, L., Nicolas, E., Saraf, K., Armaos, A., Delli Ponti, R., Izumikawa, K., Mestdagh, P. et al. (2018). SAMMSON fosters cancer cell fitness by concertedly enhancing mitochondrial and cytosolic translation. *Nat. Struct. Mol. Biol.* **25**, 1035-1046. doi:10.1038/s41594-018-0143-4

Virbasius, J. V. and Scarpulla, R. C. (1994). Activation of the human mitochondrial transcription factor A gene by nuclear respiratory factors: a potential regulatory link between nuclear and mitochondrial gene expression in organelle biogenesis. *Proc. Natl. Acad. Sci. USA* **91**, 1309-1313. doi:10.1073/pnas.91.4.1309

Vyas, S., Zaganjor, E. and Haigis, M. C. (2016). Mitochondria and Cancer. *Cell* **166**, 555-566. doi:10.1016/j.cell.2016.07.002

Wang, X. (2008). miRDB: A microRNA target prediction and functional annotation database with a wiki interface. *RNA* **14**, 1012-1017. doi:10.1261/rna.965408

Warburg, O. (1956). On the origin of cancer cells. *Science* **123**, 309-314. doi:10.1126/science.123.3191.309

Warren, E. B., Aicher, A. E., Fessel, J. P. and Konradi, C. (2017). Mitochondrial DNA depletion by ethidium bromide decreases neuronal mitochondrial creatine kinase: Implications for striatal energy metabolism. *PLoS One* **12**, e0190456. doi:10.1371/journal.pone.0190456

Yao, J., Zhou, E., Wang, Y., Xu, F., Zhang, D. and Zhong, D. (2014). microRNA-200a inhibits cell proliferation by targeting mitochondrial transcription factor A in breast cancer. *DNA Cell Biol.* **33**, 291-300. doi:10.1089/dna.2013.2132

Zhang, X., Zuo, X., Yang, B., Li, Z., Xue, Y., Zhou, Y., Huang, J., Zhao, X., Zhou, J., Yan, Y. et al. (2014). MicroRNA directly enhances mitochondrial translation during muscle differentiation. *Cell* **158**, 607-619. doi:10.1016/j.cell.2014.05.047